DEFORMATION MODES OF
COPPER-25 ATOMIC PERCENT GOLD ALLOY

A THESIS

Presented to

The Faculty and Graduate Division

by

Saghana Baran Chakrabortty

In Partial Fulfillment

of the Requirements for the Degree

Doctor of Philosophy

in the School of Chemical Engineering

Georgia Institute of Technology

January, 1974

DEFORMATION MODES OF

COPPER-25 ATOMIC PERCENT GOLD ALLOY

Approved:

Dr. Edgar A. Starke, Chairman

Date Approved Jan. 25, 1974

ACKNOWLEDGEMENTS

The author wishes to express his sincere appreciation to his thesis advisor, Dr. Edgar A. Starke, Jr., for suggesting this problem, for his helpful guidance and continuous encouragement which made this work possible. He is greatly indebted to Dr. R. F. Hochman and Dr. B. G. LeFevre for having taken time to review this work and for their constructive criticism, and to Dr. J. K. Cochran and to Dr. H. E. Grenga for their help in experimental problems encountered during this work. The discussions with Dr. C. S. Barrett and Dr. S. Mahajan while the work was in progress is gratefully appreciated.

The author is thankful to his fellow graduate students, Messrs. J. G. Rinker, T. H. B. Sanders, Jr., H. G.Paris and others, for their prompt assistance on various occasions.

The financial support of this research provided by the Air Force Office of Scientific Research, under contract Number 71-2064, is gratefully acknowledged.

TABLE OF CONTENTS

LIST OF FIGURES

Figure

LIST OF TABLES

SUMMARY

This research was conducted mainly to study the effect of ordering on the twinning modes of Cu_3Au. The ordering changes the twinning process in two ways, viz, by imposing crystallographic restrictions and by changing the stacking fault energy.

Cu_3Au single crystals with various degrees of order were deformed under uniaxial tension, with their stress axis close to a <111> direction, at 78°K and 298°K. Single crystals with various degrees of order were also deformed at 298°K under plane-strain compression, with a (110) compression plane and a $[1\bar{1}0]$ flow direction.

Disordered and partially ordered crystals were found to twin by the mode described by $K_1 = (111)$, $K_2 = (11\bar{1})$, $\eta_1 = [11\bar{2}]$, $\eta_2 = [112]$ and $s = 0.707$. The shear stress required for this mode increases with the degree of order due to crystallographic restrictions imposed by the order. Completely ordered crystals were believed to twin by the mode described by $K_1 = (111)$, $K_2 = (001)$, $\eta_1 = [\bar{1}\bar{1}2]$, $\eta_2 = [110]$ and $s = 1.414$. The twinning stress required was comparatively low because ordering lowered the stacking fault energy and did not impose any crystallographic restrictions for this mode.

CHAPTER I

INTRODUCTION

The main purpose of this research was to make an experimental and theoretical analysis of the effect of ordering on the mechanical behavior of Cu_3Au. The deformation mode of primary interest is deformation twinning. The degree of order changes the deformation characteristics of the alloy and therefore the twinning probability. These parameters influence the development of texture or preferred orientation of the alloy and this development was also analyzed. Cu_3Au has a face centered cubic (fcc) structure in the disordered state and forms an $L1_2$ structure upon ordering.

Deformation of polycrystalline fcc materials usually produces one of two kinds of textures, viz. the brass-type and the copper-type. When deformed at room temperature low stacking fault energy (SFE) materials usually develop the brass-type texture, whereas high SFE materials develop the copper-type texture. Various theories have been proposed to explain the dependence of texture on SFE (1-5).

Deformation twinning in metals and alloys has recently been reviewed by Mahajan and Williams (6). According to these authors mechanical twinning takes place whenever imposed conditions make it difficult for the material to deform by slip alone. This difficulty increases with decreasing SFE since for materials with low SFE dynamic recovery by cross slip becomes difficult, and twinning becomes more

favorable (7). Twinning also becomes favorable in this case because the separation of the partial dislocations, and thus the area of stacking faults increases with decreasing SFE.

The results obtained by various workers (8-10) indicate that ordering considerably reduces the SFE of Cu_3Au. This is a favorable factor for twinning. However, formation of twins on systems operative in the disordered state becomes difficult in the ordered state due to the crystallographic restriction imposed by the long range order; a fact that has been confirmed by observations of Laves (11) and Cahn and Coll (12). In the case of Cu_3Au, then, ordering has a favorable and an unfavorable influence on deformation twinning. This "paradox" was considered by Starke, Ogle and Sparks (13), who rolled polycrystalline Cu_3Au alloys in both the ordered and disordered conditions. They found that the texture of ordered alloys, after 42% reduction, was more analogous to that commonly produced in alloys showing the brass-type texture, whereas texture produced in the disordered alloy resembled that of pure copper. Shock loading experiments by Mikkola and Cohen (14) have shown that twins can be formed in both the disordered and the ordered states of Cu_3Au. However, the interpretation of the results of shock loading experiments is difficult because of the consecutive propagation of different waves through the specimen (6).

No extensive studies of deformation twinning and texture formation of Cu_3Au has been reported. The present study was initiated to observe the effect of order on the deformation behavior of Cu_3Au single crystals at various stages of order and to determine the contribution of deformation twinning toward the initial texture formation.

Single crystals of Cu_3Au with various degrees of order were deformed under uniaxial tension, with their stress axis close to a <111> direction, at liquid nitrogen temperature and at room temperature. A <111> direction was chosen because earlier studies have shown that fcc metals twin at lower stresses when deformed in this direction (15). Tensile tests were conducted in order to find the twinning stresses as a function of the degree of order for Cu_3Au.

Texture studies were made on Cu_3Au single crystals rolled both at room, and liquid nitrogen temperatures. These studies were used as a guide for choosing the deformation temperature for plane-strain compression studies. Cu_3Au single crystals with various degrees of order were deformed under plane-strain compression in order to study the texture development and to measure deformation twinning stresses. The compression plane of these crystals was (110) with the flow direction $[1\bar{1}0]$. Chin et al. (16) have shown that this is an easy orientation for deformation twinning to occur in fcc metals and alloys. Plane-strain compression studies were also conducted on a silver single crystal with the same orientation for comparison with Cu_3Au.

CHAPTER II

THEORY

2.1 Stacking Faults in Cu_3Au

The type of stacking fault present in Cu_3Au depends upon the degree of long range order (S) because of its effect on the dislocation structure. Unit dislocations exist in disordered Cu_3Au and also in partially ordered Cu_3Au when S is smaller than about 0.5 and the domain size is smaller than about 37 Å (17); whereas, dislocations tend to exist in pairs in Cu_3Au with larger S and domain sizes (17-22). The faults on the {111} planes of Cu_3Au with small S (0-0.5) are created by the movement of partials with a Burgers vector of a/6 $\langle 11\bar{2} \rangle$. In the case of Cu_3Au with large S, however, the neighbor relationship across the fault plane would be altered by such faulting (Figure 1a). Kear et al. (23,24) have shown that a combination of partials with a combined Burgers vector of a/3 $\langle \bar{1}\bar{1}2 \rangle$ move in the ordered $L1_2$ structure to form faults. This type of faulting is possible only when super dislocations are present in the lattice. These faults do not change the nearest neighbor relationship across the fault plane (Figure 1b). Therefore, this type of fault is more favorable in fully ordered Cu_3Au than a/6 $\langle 11\bar{2} \rangle$ faults. Both types of faults are expected to be present in an alloy with intermediate degree of order, where both unit and super dislocations exist.

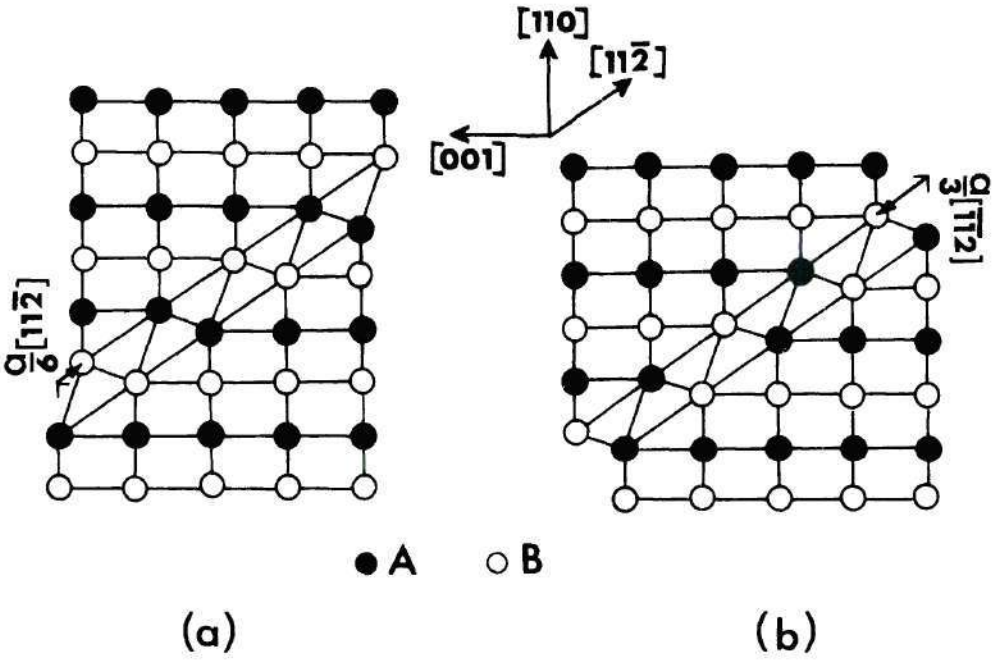

Figure 1. Faults in an Ordered Crystal (A_3B) with an $L1_2$ Structure. (The figures show a (2$\bar{2}$0) atomic plane. The entire $L1_2$ lattice is composed of two types of (2$\bar{2}$0) atomic planes stacked alternately. One kind is as shown in the figures. The other kind has all A atoms and is displaced by a/4 [112]along the plane of the paper.

(a) The fault with a/6 [$\bar{1}$12] (111) shift. There is an increase in the number like nearest neighbors across the fault plane.

(b) The fault with a/3 [$\bar{1}$12] (111) shift. The number of unlike nearest neighbors across the fault plane is same as that in the ordered lattice.)

Marcinkowski and Miller (25) postulate that the effective total SFE can be approximated by

$$SFE = E_F + S^2 E_{OR}$$

where E_F is the intrinsic SFE contribution and E_{OR} is the energy associated with the change in neighbor relationship in the fault. The value of E_F decreases with S(25). The term E_{OR} is negligible for faults with the displacement vector of $a/3 \langle 11\bar{2} \rangle$; and can be quite large for faults with the displacement vector of $a/6 \langle 11\bar{2} \rangle$; therefore, the SFE for the former is expected to decrease with S and that for the latter is not expected to decrease much, if at all. It has been reported that the SFE for Cu_3Au is 50 ergs/cm^2 when fully ordered and 150 ergs/cm^2 when disordered (10). It seems that the faults under consideration must have been the $a/3 \langle \bar{1}\bar{1}2 \rangle$ type for the fully ordered and the $a/6 \langle \bar{1}\bar{1}2 \rangle$ type for the disordered alloy.

2.2 Mechanical Twinning Modes in Cu_3Au

One or both of two twinning modes can be operative in Cu_3Au depending upon the value of S. The twinning elements $K_1 K_2 \eta_1 \eta_2$ s (6) associated with these two modes are $(111)(1\bar{1}\bar{1})\ [11\bar{2}]\ [112]\ 0.707$ and $(111)\ (001)\ [112]\ [110]\ 1.414$. Henceforth these two modes will be referred to as $a/6(111)\ [11\bar{2}]$ and $a/3(111)\ [\bar{1}\bar{1}2]$, respectively. As shown in Figure 2a, the former mode leads to a change in crystal structure of the ordered Cu_3Au. In such a case the neighbor relationships in the twin and the matrix are different. On the other hand, the latter mode does not lead to any such change (Figure 2b). The structure remains

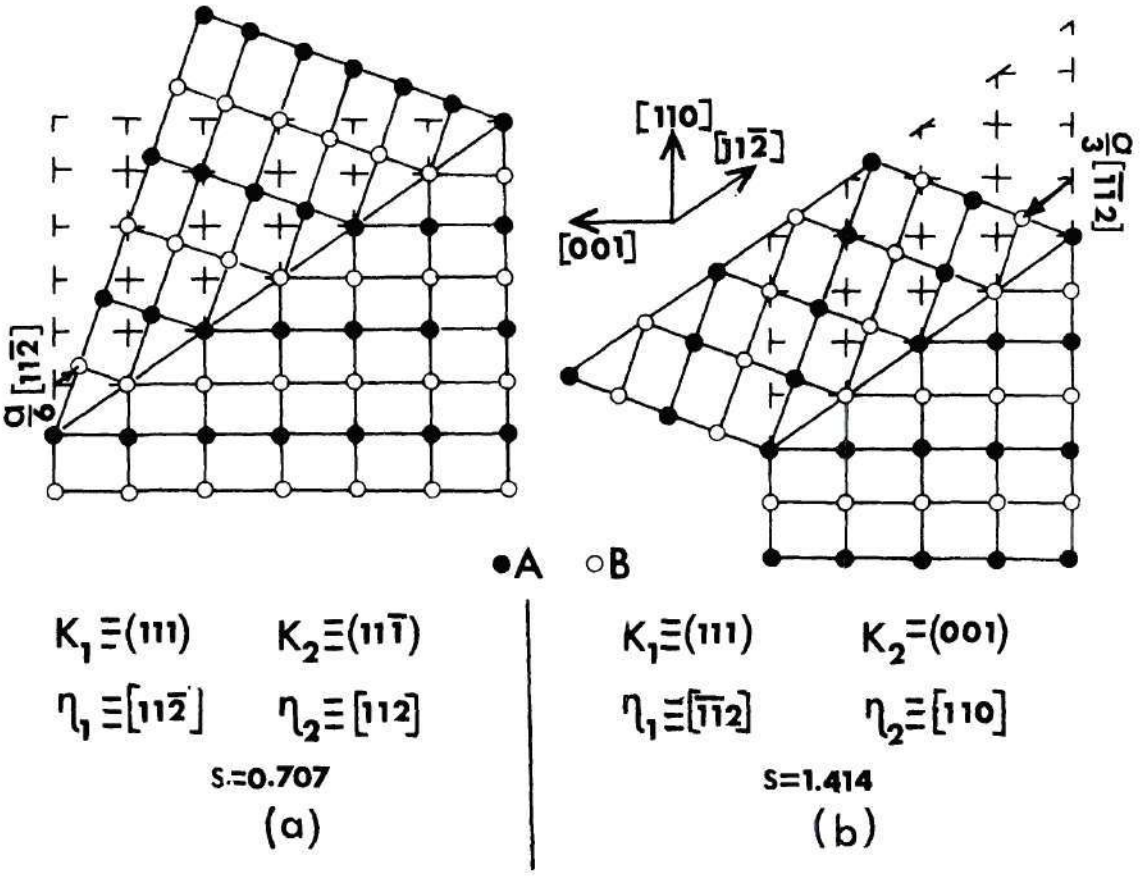

Figure 2. Twinning in an Ordered Crystal (A_3B) with an Ll_2 Structure. (The figure show a $(2\bar{2}0)$atomic plane.

(a) Twinning by the a/6 $[11\bar{2}]$ (111) Shear. Clearly, the neighbor relationship in the twin is changed.

(b) Twinning by the a/3 $[\bar{1}12]$(111) shear. No change in neighbor relationship in the twin.)

unchanged in the disordered alloy for both twinning modes. However, the $a/3\langle 11\bar{2}\rangle\{111\}$ twinning is not possible when S is zero or small because the $a/3\langle 11\bar{2}\rangle$ type faults, essential for the $a/3\langle 11\bar{2}\rangle\{111\}$ twinning (23), are absent.

The change in the nearest neighbor relationship due to $a/6(111)[11\bar{2}]$ twinning is calculated in Appendix A. The changes of unlike nearest neighbors from the matrix to the twin are given in Figure 3. As expected, the effect of these changes becomes more and more prominent as the value of S is increased, consequently, twinning by this mode is not favored in ordered Cu_3Au. As suggested by Arunachalam and Sargent (26), the $a/3[\bar{1}\bar{1}2](111)$ mode may be more favorable for the ordered alloy because it does not cause any change in neighbor relationships. The observations of twinning in Ni_3Al particles by Kear et al. (27) and Guimier and Strudel (28) support this assessment.

The structure of ordered Cu_3Au deformed by the $a/6[11\bar{2}](111)$ twinning shear is shown in Figure 4. It should be recognized that the crystal does not now have cubic symmetry; consequently, in the strictest sense this deformation should not be called twinning. The atomic arrangement in c planes shown in Figure 4 is different from those in a and b planes. There is a contraction normal to the c planes, which produces strain thereby inhibiting twinning by the $a/6[11\bar{2}](111)$ shear in the ordered alloy.

The shear stress required for twinning on the $a/6\langle 11\bar{2}\rangle\{111\}$ mode (τ_t) and for twinning on the $a/3\langle\bar{1}\bar{1}2\rangle\{111\}$ mode (τ_t') will depend on the degree of long range order, S. The value of S influences the

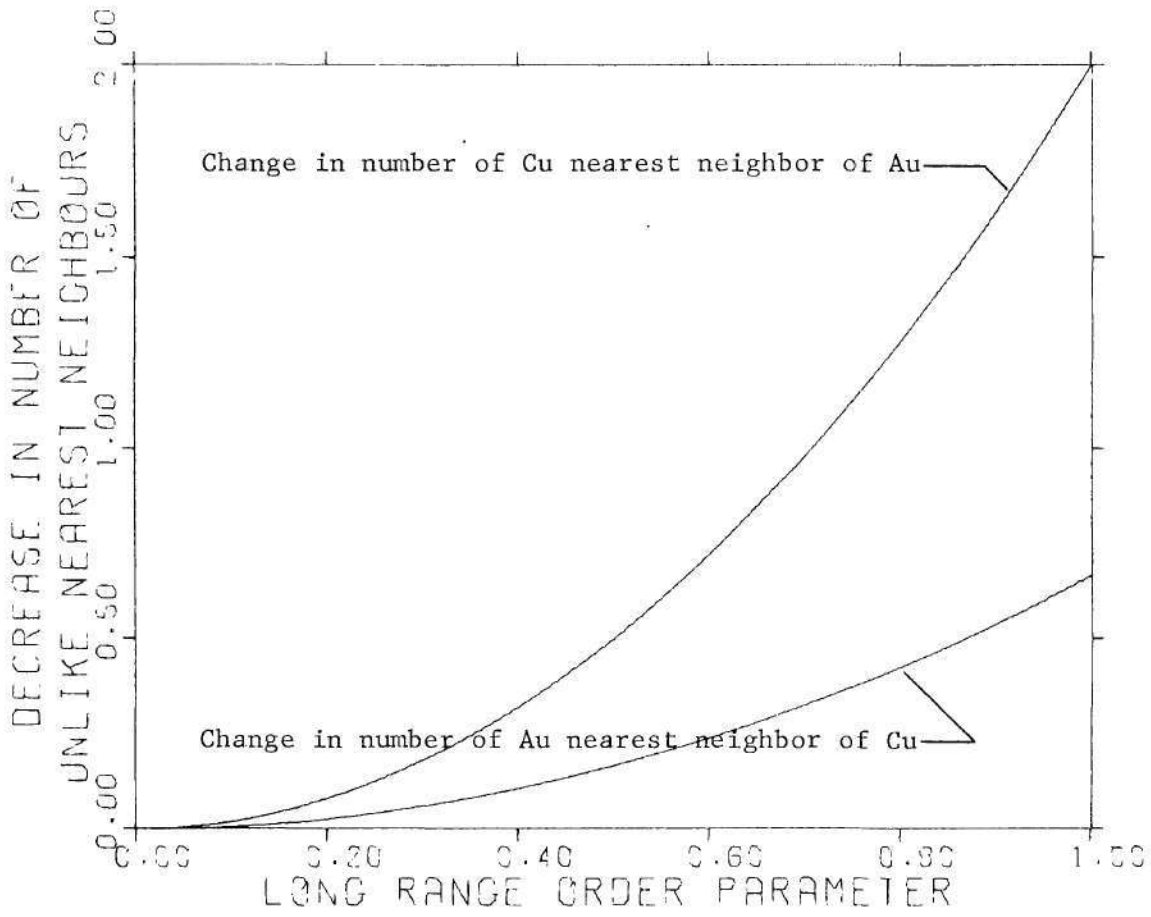

Figure 3. The change in the Average Number of Unlike Nearest Neighbors of Cu and Au Atoms in Cu Au Due to Twinning by a/6 $[11\bar{2}]$ (111) Shear,[3] with Varying Degrees of Order.

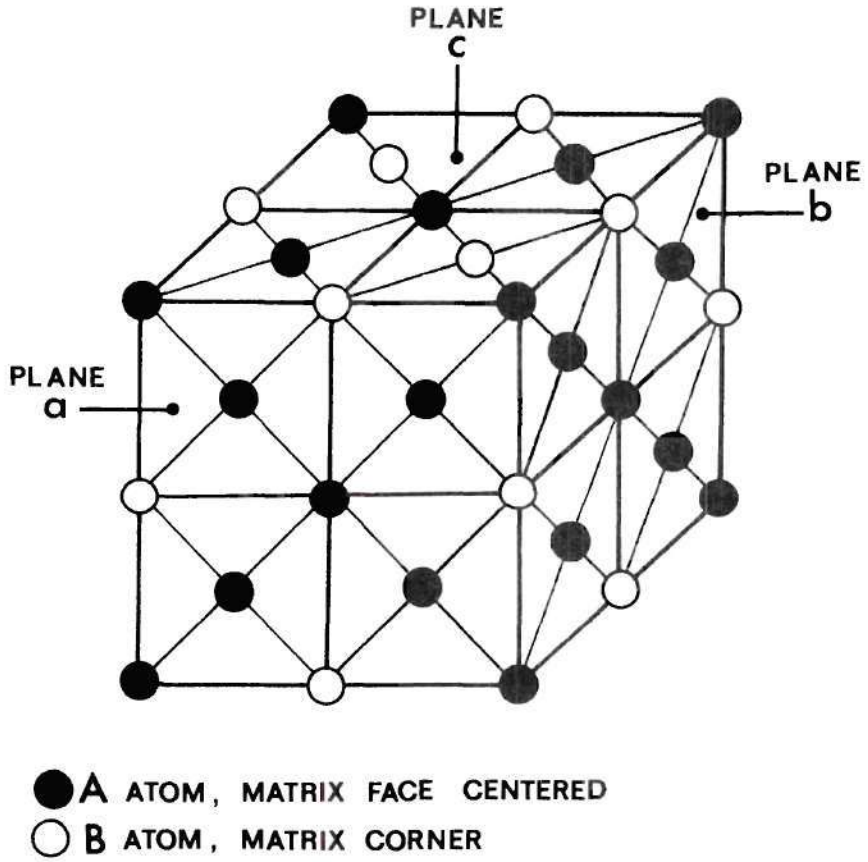

Figure 4. The Changed Ordered $L1_2$ Structure due to twinning by a/6 [112] (111) Shear. (The atomic Planes a and b are equivalent, but c is different. The structure has a tetragonal symmetry. Each a or b plane has 75 per cent Cu atoms and 25 per cent Au atoms, whereas c planes are composed of two types of atomic planes stacked alternately with one type of plane having 50 per cent Cu and 50 per cent Au atoms and other all Cu atoms. Since unlike atoms attract, the planar spacing between c planes is expected to decrease causing additional distortion in the twin.)

value of τ_t mainly by changing the neighbor relationship across the twin-matrix interface, and it influences τ_t' by decreasing the SFE for $a/3\langle\bar{1}\bar{1}2\rangle\{111\}$ faults. As a result, τ_t is expected to increase with S and τ_t' is expected to decrease.

2.3 Deformation Systems Operative Under $(110)[\bar{1}10]$ Plane Strain Compression Condition

For an arbitrary shape change in a crystal at least five shear systems need to be operative and of all the possible combinations of five or more shear systems the one which causes the minimum work will be the most favorable (29). Chin et al. (16) have incorporated deformation twinning in the Taylor analysis for fcc metals. According to their analysis, of all combinations of five or more shear systems, the one which will give the minimum value of M will be operative. M is defined as

$$M = \left(\sum_i S_i + \alpha \sum_i t_i\right)/\varepsilon,$$

where S_i = the amount of simple shear due to slip on the i-th operative system,

t_i = the amount of simple shear due to twinning on the i-th operative system,

α = the ratio of the critical resolved shear stress for twinning to that for slip,

and ε = the plastic strain.

The operative systems for an $L1_2$ alloy deformed under $(110)[\bar{1}10]$ plane strain compression can be found by similar analysis. Here in addition to $a/6\langle 11\bar{2}\rangle\{111\}$ type twinning, one has to consider the

$a/3\ \langle\bar{1}12\rangle\{111\}$ twinning.

Table 1 shows all the slip and twinning planes and directions in an $L1_2$ structure, and Figure 5(a) is the (110) standard projection showing all pertinent twinning and slip planes and directions. Figure 5(b) is an octahedron showing these systems. The octahedron is similar to that used by Chin et al. (16); the only difference being the addition of $a/3\ \langle 112\rangle\{111\}$ systems. In these figures the compression axis is the x-axis, the flow direction is the z-axis and the transverse direction is the y-axis. Thus, the imposed shape change can be described by

$$\epsilon_{yy} = 0$$

$$\epsilon_{xy} = 0$$

$$\epsilon_{xx} < 0$$

$$\epsilon_{zz} > 0.$$

Many combinations can be obtained from the above shear systems to satisfy these conditions. The combination which will be most favorable will depend upon the ratios of the resolved shear stress required for twinning to that slip. Different combinations are given below.

Case (a). Pure Slip: The systems are $S_{\bar{1}}$, S_2, $S_{\bar{4}}$, S_5, S_7, $S_{\bar{8}}$, S_{10}, $S_{\bar{11}}$. From the analysis by Chin et al.(16), $S_{\bar{1}} = S_2 = S_{\bar{4}} = S_5 = S_7 = S_{\bar{8}} = S_{10} = S_{\bar{11}} = -\frac{\sqrt{6}}{4}\ \epsilon_{xx}$, and $M = 2\sqrt{6}$.

Case (b). Mixed Slip and Twinning by the $a/6\ \langle 112\rangle\{111\}$ mode. The slip systems are $S_{\bar{1}}$, S_2, $S_{\bar{4}}$, S_5. The twinning systems are t_9 and t_{12}. From the analysis of Chin et al.(16), $S_{\bar{1}} = S_2 = S_{\bar{4}} = S_5 = -\frac{\sqrt{6}}{4}\ \epsilon_{xx}$, $t_9 = t_{12} = -\frac{3\sqrt{2}}{4}\ \epsilon_{xx}$, and $M = \sqrt{6} + \frac{3\sqrt{2}}{2}\ \alpha$. $\alpha = \frac{\tau_t}{\tau_s}$; τ_t and τ_s are

Table 1. Shear Systems to be Considered for an Alloy of the $L1_2$ System.

The Twelve Slip Systems												
Plane	(111)			$(1\bar{1}\bar{1})$			$(\bar{1}11)$			$(\bar{1}\bar{1}\bar{1})$		
Direction	$01\bar{1}$	$\bar{1}01$	$1\bar{1}0$	011	$\bar{1}0\bar{1}$	$1\bar{1}0$	$01\bar{1}$	101	$\bar{1}\bar{1}0$	011	$10\bar{1}$	$\bar{1}\bar{1}0$
System	S_1	S_2	S_3	S_4	S_5	S_6	S_7	S_8	S_9	S_{10}	S_{11}	S_{12}

The Twelve $a/6\{111\}\langle 112\rangle$ Twinning Systems												
Plane	(111)			$(1\bar{1}\bar{1})$			$(\bar{1}11)$			$(\bar{1}\bar{1}\bar{1})$		
Direction	$\bar{2}11$	$1\bar{2}1$	$11\bar{2}$	$\bar{2}1\bar{1}$	$1\bar{2}\bar{1}$	112	211	$\bar{1}2\bar{1}$	$\bar{1}1\bar{2}$	$21\bar{1}$	$\bar{1}2\bar{1}$	$\bar{1}12$
System	t_1	t_2	t_3	t_4	t_5	t_6	t_7	t_8	t_9	t_{10}	t_{11}	t_{12}

The Twelve $a/3\{111\}\langle 112\rangle$ Twinning Systems												
Plane	(111)			$(1\bar{1}\bar{1})$			$(\bar{1}11)$			$(\bar{1}\bar{1}\bar{1})$		
Direction	$\bar{2}\bar{1}\bar{1}$	$\bar{1}2\bar{1}$	$\bar{1}\bar{1}2$	$2\bar{1}\bar{1}$	$\bar{1}21$	$\bar{1}\bar{1}2$	$\bar{2}11$	$12\bar{1}$	$1\bar{1}2$	$\bar{2}\bar{1}1$	121	$\bar{1}\bar{1}2$
System	t'_1	t'_2	t'_3	t'_4	t'_5	t'_6	t'_7	t'_8	t'_9	t'_{10}	t'_{11}	t'_{12}

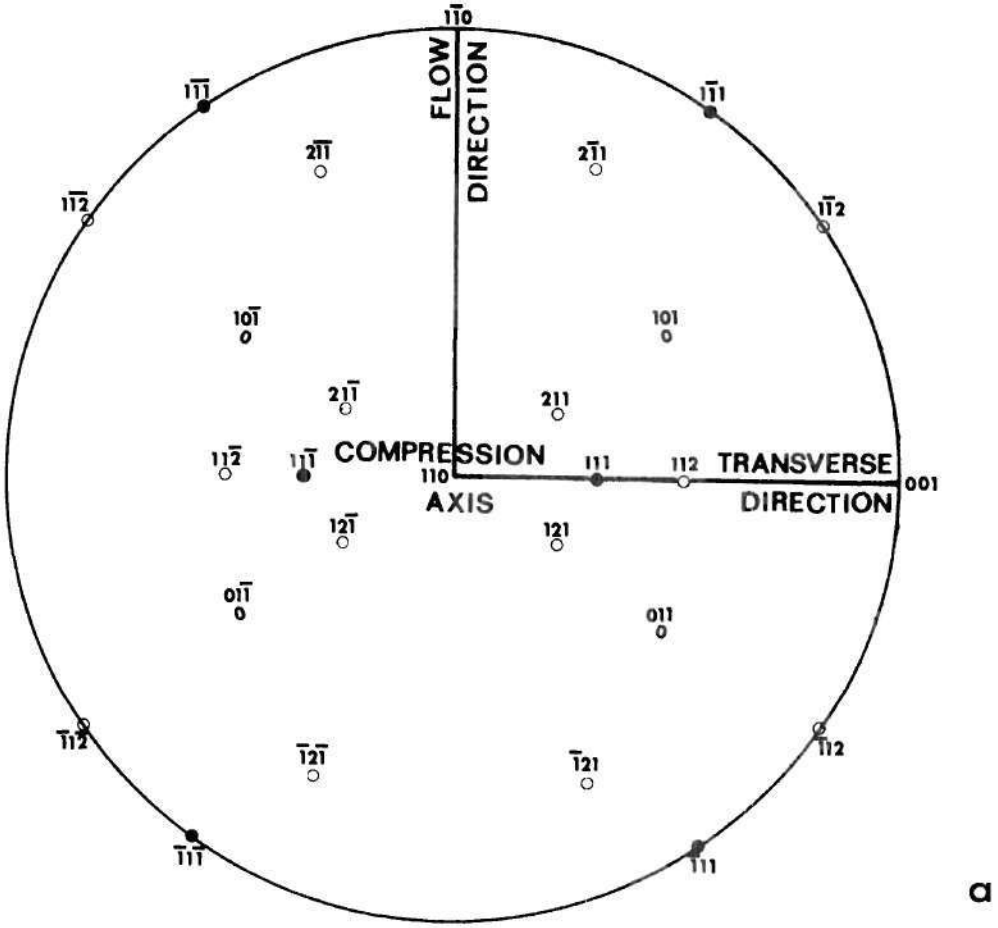

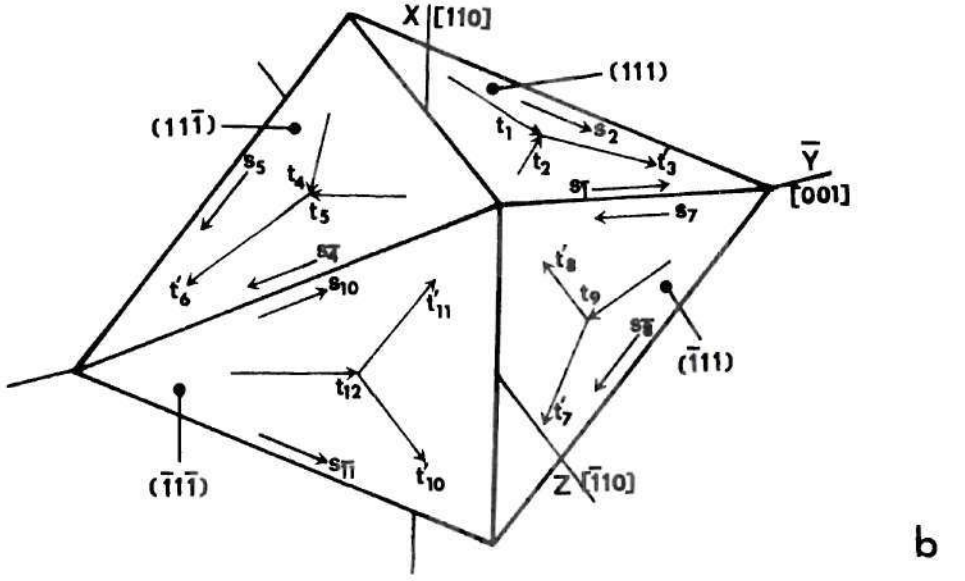

Figure 5. (a) (110) Stereographic Projections Showing the Planes and Directions of the Systems Favorable Under (110) $[1\bar{1}0]$ Plane-Strain Compression of Cu_3Au.
(b) Octahedrom Showing the Possible Shear Systems to be Activated by (110) $[1\bar{1}0]$ Plane-Strain Compression.

the resolved shear stress for twinning by the a/6<112>{111} mode and slip respectively.

Case (c). Mixed Slip and Twinning by the a/3 <112>{111} Mode. The slip systems are S_7, $S_{\bar{8}}$, S_{10}, $S_{\bar{11}}$. The twinning systems are t_3' and t_6'.

$$\epsilon_{xx} = -\frac{\sqrt{2}}{3}\,(t_3' + t_6')$$

$$\epsilon_{yy} = \frac{\sqrt{2}}{3}\,(t_3' + t_6') - \frac{1}{\sqrt{6}}\,(S_7 + S_{\bar{8}} + S_{10} + S_{\bar{11}}) = 0 \qquad 2.3.1$$

$$\epsilon_{xy} = -\frac{1}{6}\,(t_3' - t_6') - \frac{1}{4\sqrt{3}}\,(S_7 - S_{\bar{8}} - S_{10} + S_{\bar{11}}) = 0$$

From symmetry considerations $t_3' = t_6'$ and $S_7 = S_{\bar{8}} = S_{10} = S_{\bar{11}}$. Hence the solution to equations 2.3.1 is

$$t_3' = t_6' = -\frac{3\sqrt{2}}{4}\,\epsilon_{xx}$$

and

$$S_7 = S_{\bar{8}} = S_{10} = S_{\bar{11}} = -\frac{\sqrt{6}}{4}\,\epsilon_{xx}$$

Then,

$$M = \left(\sum_i S_i + \alpha' \sum_i t_i'\right)/\epsilon_{xx}$$

$$= 6 + \frac{3\sqrt{2}}{2}\,\alpha'$$

$\alpha' = \frac{\tau_{t'}}{\tau_s}$; τ_t' and τ_s are the resolved shear stress for twinning by the a/3 <112>{111} mode and slip, respectively.

Case (d). Mixed Twinning by the a/6 <112>{111} and a/3 <112>{111} modes. The systems are t_9, t_{12}, t_3', and t_6'.

Here,

$$\epsilon_{xx} = -\sqrt{2}/3\,(t_3' + t_6')$$

$$\epsilon_{yy} = \sqrt{2}/3\,(t_3' + t_6' - t_9 - t_{12}) = 0 \qquad 2.3.2$$

$$\epsilon_{xy} = -1/6\,(t_3' - t_6') = 0$$

From symmetry considerations $t_3' = t_6'$ and $t_9 = t_{12}$. Hence from Equation 2.3.2

$$t_3' = t_6' = t_9 = t_{12} = -\frac{3\sqrt{2}}{4}\ \epsilon_{xx}$$

and

$$M = (\alpha' \sum_i t_i' + \alpha \sum_i t_i)/\epsilon_{xx} = \frac{3\sqrt{2}}{2}\ \alpha + \frac{3\sqrt{2}}{2}\ \alpha'$$

It should be noted that not more than four systems are operative in this case, apparently contradicting the theory that for an arbitrary shape change at least five systems have to be simultaneously operative. However, if the imposed shape change is produced and the minimum work criterion is satisfied, this combination should be favored over all others.

Case (e). Pure Twinning by the a/6 <112>{111} mode.

The systems are t_1, t_2, t_4, t_5, t_9, t_{12}. From the analysis of Chin et al. (16)

$$t_1 = t_2 = t_4 = t_5 = t_9 = t_{12} = -\frac{3\sqrt{2}}{4}\ \epsilon_{xx},$$

and

$$M = \frac{9\sqrt{2}}{2}\ \alpha$$

Case (f). Pure Twinning by a/3 <112>{111} mode.

The Systems are t_3', t_6', t_7', t_8', t_{10}', t_{11}'.

Here

$$\epsilon_{xx} = -\frac{2\sqrt{3}}{3}\ (t_3' + t_6')$$

$$\epsilon_{yy} = \sqrt{2}/3\ (t_3' + t_6') - \sqrt{2}/6(t_7' + t_8' + t_{10}' + t_{11}') = 0 \qquad 2.3.3$$

$$\epsilon_{xy} = -1/6\ (t_3' - t_6') + 1/4(t_7' - t_8' - t_{10}' + t_{11}') = 0$$

From symmetry considerations

$$t_3' = t_8' \quad \text{and} \quad t_7' = t_8' = t_{10}' = t_{11}'.$$

From equations 2.3.3 we obtain

$$t_3' = t_6' = t_7' = t_8' = t_{10}' = t_{11}' = -\frac{3\sqrt{2}}{4}\ \epsilon_{xx}$$

and

$$M = \alpha' \sum_i t_i' / \epsilon_{xx} = \frac{9\sqrt{2}}{2}\ \alpha'.$$

The conditions for which one case will be favored over the other can be found from the criterion of minimum M. These conditions are given in Table 2. Since in the disordered alloy, and in the alloy with low S, a/3 $\langle\bar{1}\bar{1}2\rangle\{111\}$ twinning does not occur, only cases (a), (b) and (e) are possible.

The values of τ_s will increase with deformation and the values of α and α' will decrease, and when the value of α or α' is low enough, deformation twinning will occur. Therefore, it is expected that at different stages of deformation different cases will be operative. The critical values of α and α', given in Table 2, should be modified if the original orientation of the crystal changes during deformation.

2.4 Rotation of the Crystal Deformed Under (110) $[1\bar{1}0]$ Plane Strain Compression due to Shear on a/6 $\langle 11\bar{2}\rangle\{111\}$ Systems

The systems on which a/6 $\langle 11\bar{2}\rangle\{111\}$ shear mode is most favorable are $[11\bar{2}](\bar{1}\bar{1}\bar{1})$ and $[\bar{1}\bar{1}2](\bar{1}11)$. Considering bi-axial stress systems for the plane-strain compression, the Schmidt factor is given by

Table 2. Combinations of Shear Systems Which can be Operative When an Alloy of the $L1_2$ System Undergoes Plane Strain Compression with a (110) Compression Plane and a $[1\bar{1}0]$ Flow Direction.

Combination	Systems	M	Condition
a	$S_{\bar{1}}$, S_2, $S_{\bar{4}}$, S_5 S_7, $S_{\bar{8}}$, S_{10}, $S_{\overline{11}}$	$2\sqrt{6}$	$\alpha > \frac{2}{\sqrt{3}}$, $\alpha' > \frac{2}{\sqrt{3}}$
b	$S_{\bar{1}}$, S_2, $S_{\bar{4}}$, S_5 t_9, t_{12}	$\sqrt{6} + \frac{3\sqrt{2}}{2}\alpha$	$\alpha < \frac{2}{\sqrt{3}}$, $\alpha' > \frac{2}{\sqrt{3}}$
c	$S_{\bar{1}}$, $S_{\bar{8}}$, S_{10}, $S_{\overline{11}}$, t'_3, t'_6	$\sqrt{6} + \frac{3\sqrt{2}}{2}\alpha'$	$\alpha > \frac{2}{\sqrt{3}}$, $\alpha' < \frac{2}{\sqrt{3}}$
d	t_9, t_{12} t'_3, t'_6	$\frac{3\sqrt{2}}{2}\alpha + \frac{3\sqrt{2}}{2}\alpha'$	$\alpha < \frac{2}{\sqrt{3}}$, $\alpha' < \frac{2}{\sqrt{3}}$
e	t_1, t_2, t_4, t_5 t_9, t_{12}	$\frac{9\sqrt{2}}{2}\alpha$	$\alpha < \frac{1}{\sqrt{3}}$, $\alpha' > 2\alpha$
f	t'_3, t'_6, t'_7, t'_8, t'_{10}, t'_{11}	$\frac{9\sqrt{2}}{2}\alpha'$	$\alpha > 2\alpha'$, $\alpha' < \frac{1}{\sqrt{3}}$

$$m = (\cos \phi_t \cos \lambda_t + \cos \phi_c \cos \lambda_c)$$

where ϕ_t and λ_t are the angles made by the flow direction with the slip plane normal and the slip direction, respectively, and ϕ_c and λ_c are the angles made by the compression direction with the same elements.

The value of m is the same for both the $[\bar{1}12](\bar{1}1\bar{1})$ and $[\bar{1}1\bar{2}](\bar{1}11)$ systems for the orientation under consideration. If one region of the crystal shears to a larger extent on the $[\bar{1}12](\bar{1}1\bar{1})$ system, then the $[\bar{1}12]$ direction will rotate toward the flow direction and the $[\bar{1}1\bar{1}]$ direction will rotate toward the compression axis. The net rotation of the {111} planes is shown in Figure 6. These rotations will initially increase m for the $[\bar{1}12](\bar{1}1\bar{1})$ system and decrease m for the $[\bar{1}1\bar{2}](\bar{1}11)$ system. Therefore, the initial rotation of this region of the crystal will not be corrected by the rotation in the opposite direction by more shear on the complementary system. The $[\bar{1}12](\bar{1}1\bar{1})$ system will be more active until extensive rotation produces equal values of m for both systems. At this point both systems will be active and no further rotation will occur. However, it is quite possible that other systems might become more favorable before this point is reached.

Similarly, other regions of the crystal might undergo deformation on other possible a/6 $\langle 11\bar{2}\rangle\{111\}$ systems, viz. $[1\bar{1}\bar{2}](1\bar{1}1)$, $[\bar{1}1\bar{2}](\bar{1}11)$ and $[1\bar{1}2](1\bar{1}1)$. Rotations resulting from these shear systems are indicated by arrows in Figure 6. Since the a/6 $\langle 11\bar{2}\rangle\{111\}$ shear is less favorable in the ordered alloy, rotation due to shear of this type is expected to occur only after high deformation, when order is reduced and large stresses are reached.

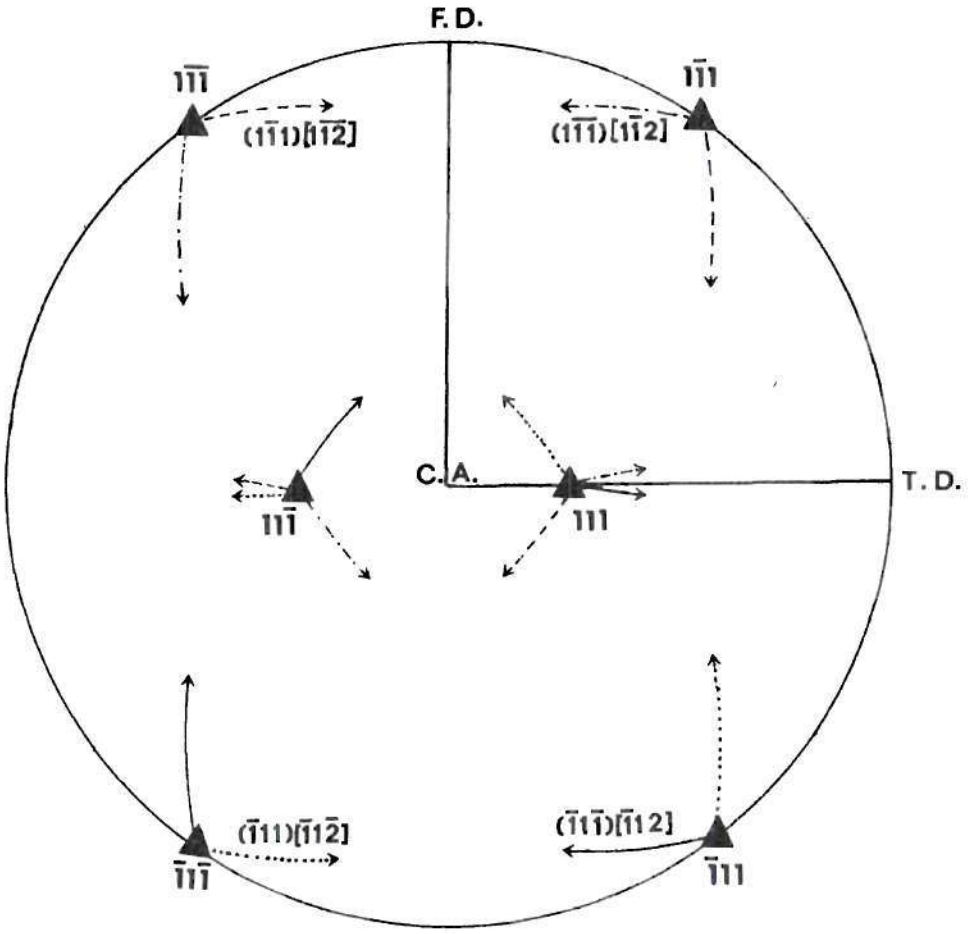

Figure 6. The Rotation of a Crystal Deformed under $(110)\ [1\bar{1}0]$ Plane-Strain Compression due to $1/6\ \langle 11\bar{2}\rangle\{111\}$ Type of Shear. (The initial positions of the $\{111\}$ poles are shown by the triangles and the rotation of these poles are indicated by arrows. The solid arrows indicate rotation due to extensive deformation on the $(\bar{1}1\bar{1})[\bar{1}12]$ system. Other arrows are labelled accordingly. The length (angular) of an arrow is proportional to the amount of rotation of the corresponding pole.)

2.5 Twinning Matrices

Matrices for Planes and Directions of Twins

The directions (and planes) in the matrix and twin are related in such a way that the indices of a direction in the matrix, when operated on by the twinning matrix, will produce the indices of the same direction in the twin and vice versa. There is one such twinning matrix for each twin plane. The matrices for twinning on (111), $(\bar{1}11)$, $(1\bar{1}1)$ and $(11\bar{1})$, as given by Mahajan (30) are as follows.

$$\frac{1}{3}\begin{vmatrix} \bar{1} & 2 & 2 \\ 2 & \bar{1} & 2 \\ 2 & 2 & \bar{1} \end{vmatrix}; \quad \frac{1}{3}\begin{vmatrix} \bar{1} & \bar{2} & \bar{2} \\ \bar{2} & \bar{1} & 2 \\ \bar{2} & 2 & \bar{1} \end{vmatrix}; \quad \frac{1}{3}\begin{vmatrix} \bar{1} & \bar{2} & 2 \\ \bar{2} & \bar{1} & \bar{2} \\ 2 & \bar{2} & \bar{1} \end{vmatrix}; \text{ and } \frac{1}{3}\begin{vmatrix} \bar{1} & 2 & \bar{2} \\ 2 & \bar{1} & \bar{2} \\ \bar{2} & \bar{2} & \bar{1} \end{vmatrix}$$

These matrices depend only on the twin plane and not on the shear vector.

Matrices for Change in a Direction due to Twinning

When a crystallographic direction is homogeneously sheared by a twin, its direction and magnitude are changed except for the directions lying on the K_1 plane. The change can be assessed by operations on the different directions by a matrix. The operational matrix not only depends upon the twin plane, but also on the twinning shear. Thus the operational matrices for changes in crystallographic directions by twinning on a (111) plane by a/6 $[\bar{2}11]$ shear and a/3 $[\bar{1}\bar{1}2]$ shear are given by

$$\frac{1}{6}\begin{vmatrix} 4 & \bar{2} & \bar{2} \\ 1 & 7 & 1 \\ 1 & 1 & 7 \end{vmatrix} \text{ and } \frac{1}{3}\begin{vmatrix} 2 & \bar{1} & \bar{1} \\ \bar{1} & 2 & \bar{1} \\ 2 & 2 & 5 \end{vmatrix} \text{ respectively.}$$

Changes in the Miller indices of a crystallographic plane by twinning can be obtained from a knowledge of the change in indices of nonparallel directions lying on that plane. For example, using the above matrix one can find that a/6 $[\bar{2}11](111)$ twinning will change $[\bar{1}10]$, $[011]$ and $[112]$ directions to $[\bar{1}10]$, 1/3 $[\bar{2}17]$ amd 1/3 $[\bar{1}\ \bar{1}\ 14]$, respectively. The former three directions lie in the $(\overline{11}1)$ plane and the latter three lie in the (771) plane; thus, an $(\overline{11}1)$ crystallographic plane in the matrix, when sheared homogenously by a/6 $[\overline{11}2](111)$ twinning, will transform to a crystallographic plane with the indices (771) with respect to matrix coordinates.

CHAPTER III

EXPERIMENTAL

The Cu_3Au alloy for this work was made from high purity copper and gold (99.999+ weight percent) by vacuum induction melting. The alloy was remelted numerous times to ensure proper mixing. Part of this alloy was swaged into rods from which single crystals of about 4 mm diameter were grown by a modified Bridgman technique using high purity graphite molds. The remainder of the alloy was rolled into bars, about 12.5 mm x 2.5 mm, and flat single crystals were grown from these bars, also by the modified Bridgman technique. The orientations of the crystals were controlled by using seed crystals. The crystals were homogenized at 900°C for one week, cooled to 450°C and quenched in iced brine. A flat silver single crystal was also grown from high purity silver in a high purity graphite mold.

Specimens were cut from the single crystals by the spark-erosion technique and finishing was done by electropolishing (31). The Cu_3Au crystals were heat treated in vacuo to different degrees of order. The heat-treatments, long range order parameters, and the average ordered domain sizes are given in Table 3.

Small disks parallel to (220) planes were cut from the single crystals and electropolished to remove any deformed surface layer. The (110) and (220) diffraction peaks were then measured with a diffractometer using Cu-K_α radiation. The long range order parameters were

Table 3. Long Range Order Parameters and Average Domain Sizes of Heat Treated Cu_3Au Single Crystals. (TN and T Indicate that the Specimens were pulled under uniaxial tension at 78°and 298°K respectively. R indicates that the specimen was rolled and CM Indicates that the sample was deformed under plane-strain compression.)

Sample Numbers	Heat Treatment	Order Parameter, S	Average Domain Size $< D_{110} >$
T15, CM1, R1	Quenched from 450°C	0	
T16, CM2, R2	Quenched-annealed at 275°C for 1 hr-Quenched	0.5	30 Å
CM3, R3	Quenched-heated to 350°C-cooled to 250°C in 4 days-furnace cooled.	0.8	135 Å
T8	Quenched-heated to 350°C-cooled to 200°C in 6 days-furnace cooled.	0.9	260 Å
TN9, T10, T12 T17, CM4, R4, CM6	Quenched-heated to 380°C-cooled to 150°C in two weeks-furnace cooled.	1	(500 Å)*

*The domain size for R4 and CM4 is about 500 Å. The rest of the alloys in this group have too large domain sizes to be measured with good accuracy.

determined from integrated intensities (32), and the average ordered domain sizes were calculated from peak breadths (33).

Tensile samples were prepared from 4mm diameter single crystal rods. A gage section, about 15 mm long, was reduced to about 3 mm in diameter by a combination of spark machining and electropolishing. A fine pointed platinum cathode was used for electropolishing to avoid enhanced dissolution at the ends of the gage section. The orientation of these crystals is given in Figure 7. Crystals were deformed under uniaxial tension at both liquid nitrogen temperature ($78^{o}K$) and room temperature ($298^{o}K$) at a strain rate of 10^{-3}/second using an Instron testing machine.

Flat single crystals were cut and polished to about 6 mm x 10 mm x 2.5 mm for rolling studies. The (110) rolling plane was about 6 mm x 10 mm with the longitudinal axis parallel to the $[\bar{1}10]$ rolling direction (Figure 8). One set of crystals was immersed in liquid nitrogen for a sufficient time to ensure that the crystals reached $\sim 78^{o}K$, immediately after which they were rolled, with a thickness reduction of about 8.3 percent per pass. The procedure was repeated until the total reduction was about 25 percent. The (111) pole figures were determined on these samples by the Schulz technique utilizing a Siemens texture goniometer. These measurements were repeated after 50 percent and 75 percent reduction in thickness. Similar studies were done at room temperature, using another set of crystals.

Flat single crystals were cut and polished to about 12.5 mm x 10 mm x 2.5 mm for plane-strain compression studies. The (110) compression

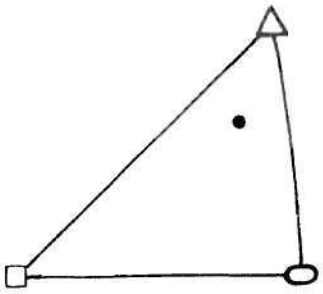

Figure 7. The Orientation of the Single Crystals Used for the Uniaxial Tension Tests.

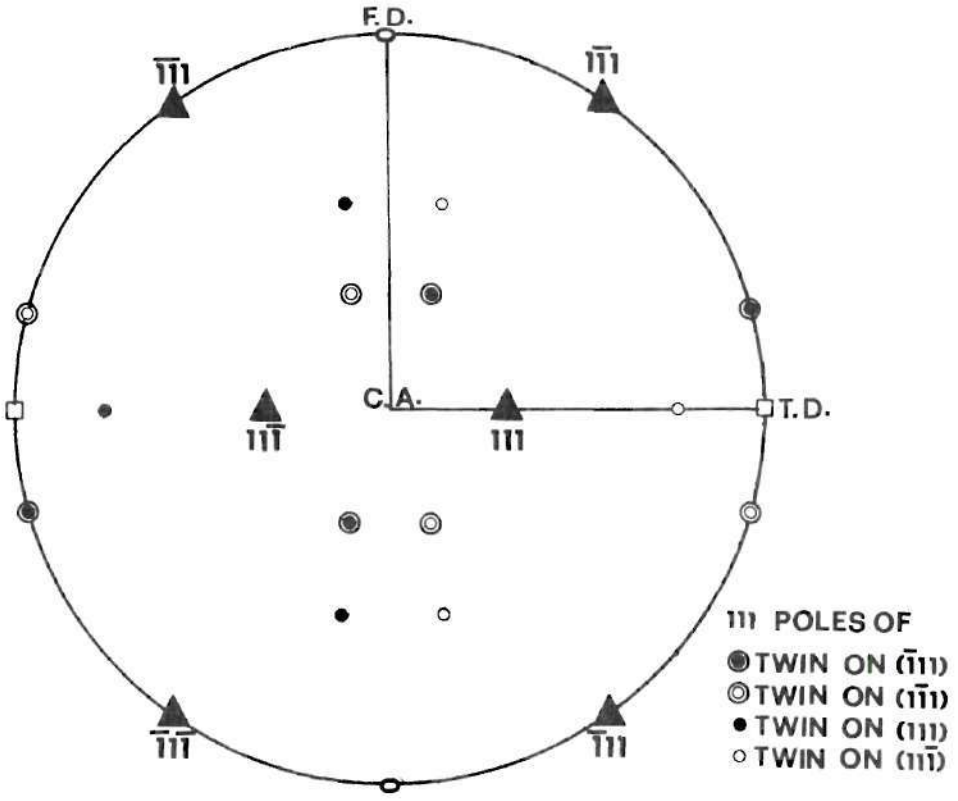

Figure 8. The Standard Projection of the Cu_3Au Single Crystals Used for Rolling and Plane-Strain Compression Studies. (The figure also shows positions of $\{111\}$ poles of twins).

plane was about 12.5 mm x 10 mm. The crystals were about 10 mm long parallel to the $[1\bar{1}0]$ flow direction (Figure 8). These samples were deformed under plane-strain compression at a strain rate of approximately 3×10^{-3}/second, using a device described by Chin et al. (34). The surface of the crystals were covered with a 0.08 mm thick teflon sheet to reduce frictional effects. At various stages of deformation, the surfaces were examined for slip lines and twin bands, with an optical microscope. In addition, texture measurements were made, and transmission electron microscopy was performed on these crystals. Similar plane-strain compression studies were also performed on the silver crystal for comparison.

CHAPTER IV

RESULTS AND DISCUSSION

4.1 Tensile Tests

No load drops or crackling noises, both of which are characteristics of mechanical twinning, were observed when the crystals were deformed under uniaxial tension at 78°K. Optical microscopy, however, showed some evidence of deformation twins (Figure 9) in the completely ordered crystals. There was no information available for assessment of the twinning stress. Since the boiling liquid nitrogen prohibited detection of the "twinning sounds", a similar set of single crystals were deformed at room temperature (298°K). Crackling noises due to deformation twinning were heard only during the initial stages of deformation of the three fully ordered samples. The onset and the end of twinning are shown on the shear-stress versus shear-strain curve of a fully ordered specimen in Figure 10. On the same figure the shear-stress versus shear-strain curves for Cu_3Au alloys with other values of S are also shown. Figure 11 shows the variation of yield stress and work hardening rate (θ_{II}) with the degree of long range order.

These results may be briefly explained using the previous studies reviewed in reference 17. The passage of unit dislocations across a slip plane of the disordered alloy partially destroys the local order (35,36) and increases yield stress. The unit dislocations must also cut through the small long range ordered domains for flow (25) in Cu_3Au

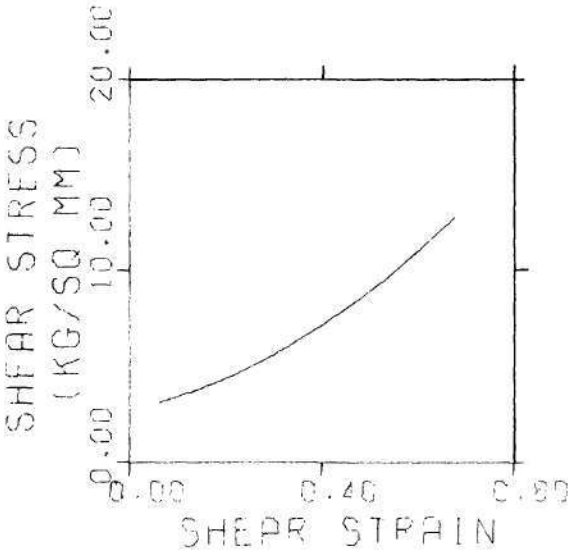

(a)

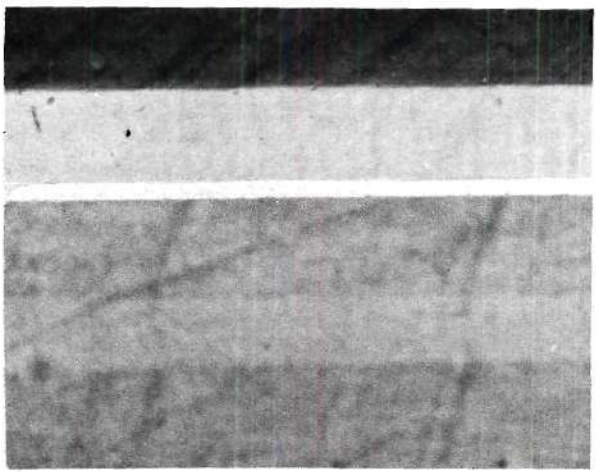

(b)

(c)

Figure 9. (a) Shear Stress-Shear Strain Curve of Ordered Cu_3Au Deformed under Uniaxial Tension at $78^{o}K$.

(b) A Twin Band on the Surface of the Crystal (unpolished). The Band Itself is Deformed Internally. Magnification 300X.

(c) A Similar Twin Band After it was Polished and Etched with a 50:50 Mixture of 10 Percent KCN and 10 Percent $(NH_4)_2 S_2O_8$. Magnification 300X.

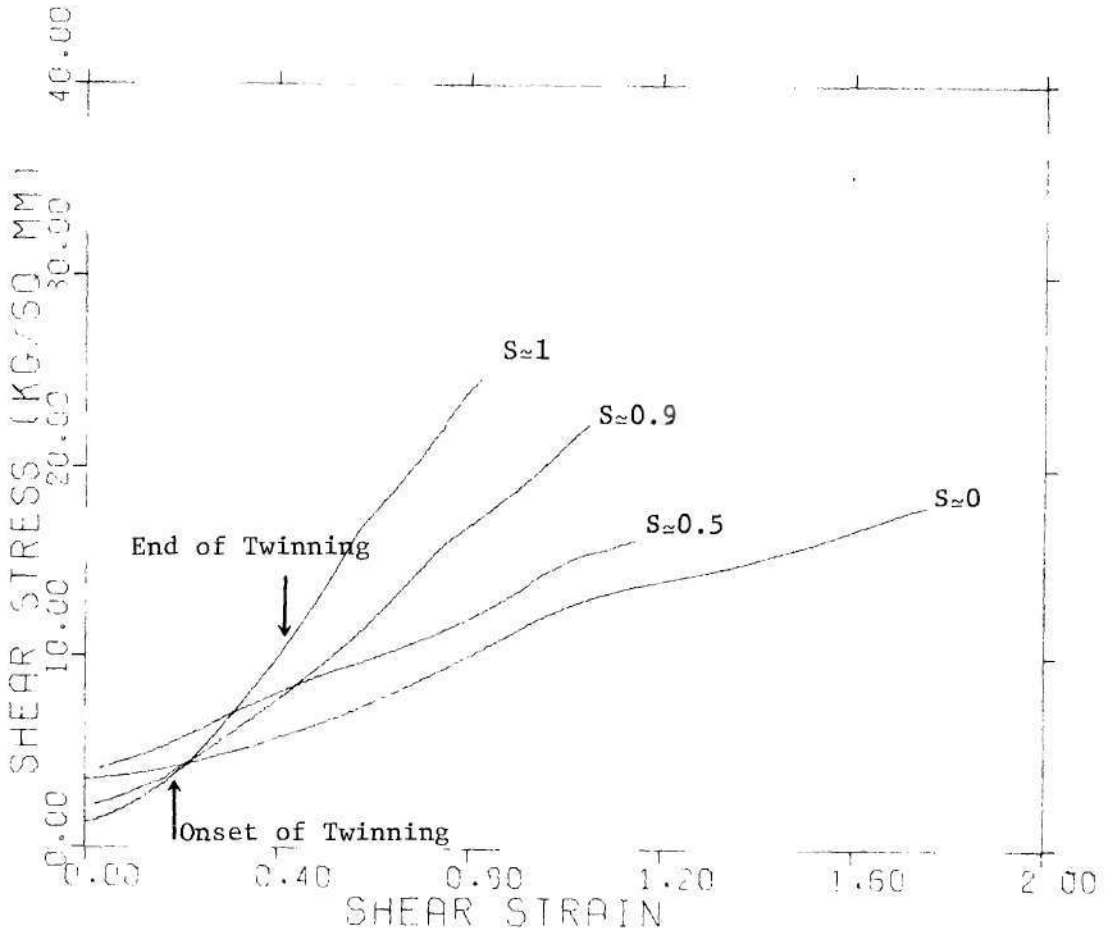

Figure 10. The Resolved Shear Stress - Resolved Shear Strain Curves of Cu_3Au with Various Degrees of Long Range Order, Deformed Under Uniaxial Tension at $298^{o}K$ with a Strain Rate of Approximately 1×10^{-3}.

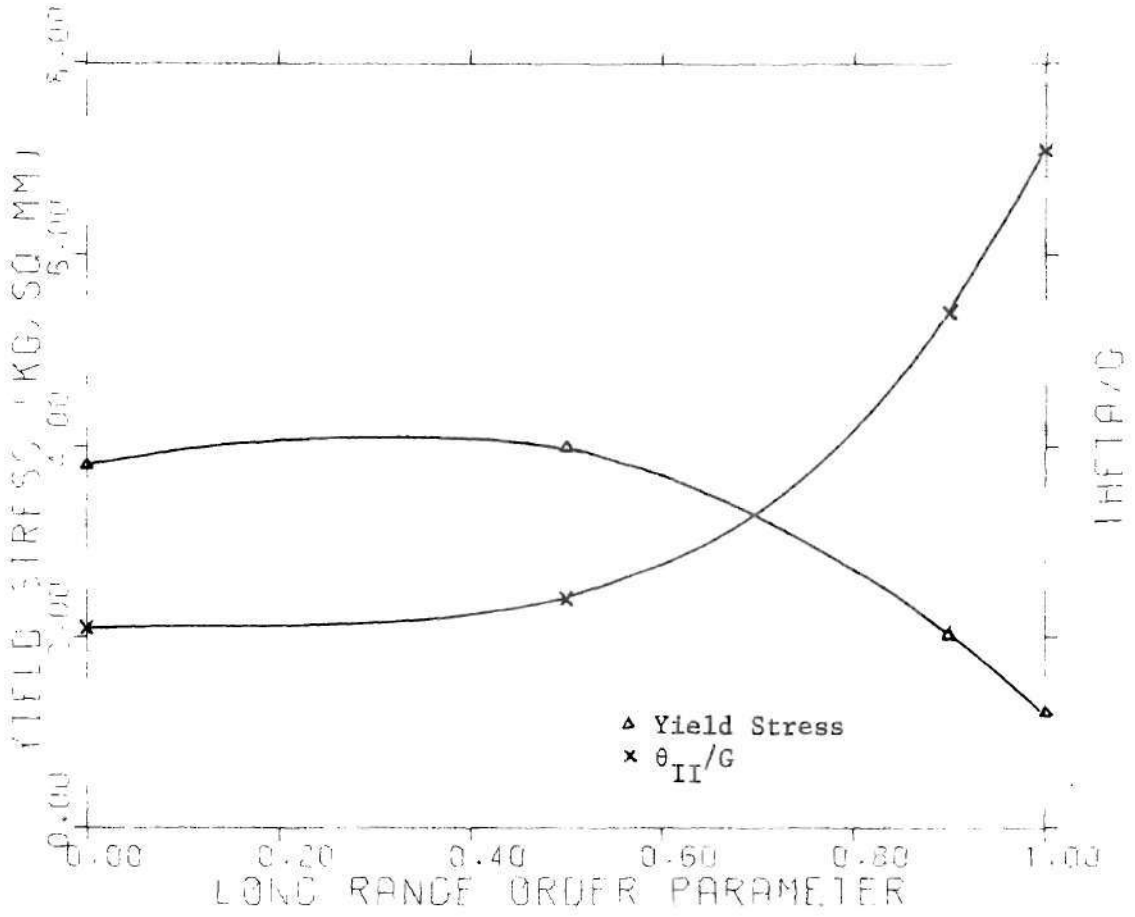

Figure 11. The Second Stage Work Hardening Rate (θ_{II}) and the Yield Stress of Cu_3Au with Various Degrees of Order Deformed Under Uniaxial Tension at 298°K.

with S $\simeq$ 0.5, causing a slightly greater increase in yield stress. When S and domain size are larger, the dislocations tend to move in pairs, with the proportion of mobile super dislocations increasing with S (17). Since the passage of super dislocations does not destroy the long range order on the average, the yield stress decreases as S approaches unity.

The value of θ_{II} is almost the same for the Cu_3Au specimens with S $\simeq$ 0 and S $\simeq$0.5, whereas it increases substantially for the specimens with S $\simeq$0.9 and S $\simeq$1. Previous workers (18-21) explained the increase in θ_{II} in terms of interactions of the super dislocations. For example, Davis and Stoloff (18) have suggested that the strain hardening of ordered Cu_3Au is due to a source exhaustion mechanism. As a super dislocations expands from its source on a slip plane, there is a finite probability that the screw component will cross-slip to another (111) plane creating an antiphase boundary on a cube plane. If the cross-slip occurs a barrier for expansion of other loops from the source will be created, because any further movement of either of these dislocations would increase the antiphase boundary area. Eventually the source becomes ineffective, resulting in the observed hardening.

The twinning starts at a very low stress level for the completely ordered Cu_3Au alloy. The twinning mode in this case is believed to be a/3 $\langle\bar{1}12\rangle$ $\{111\}$, since the stress required for twinning by the a/6 $\langle11\bar{2}\rangle$ $\{111\}$ mode is considerably higher, as shown by the plane-strain compression results (Section 4.3) In this case the highest stressed $\{111\}$ $\langle\bar{1}12\rangle$ system is (111) $[\bar{1}12]$. The resolved shear stress on this system, at the onset of twinning, is about 2.6 kg/mm^2. The SFE of fully ordered

Cu_3Au is 50 kg/cm^2 (10). From the results presented by Venables (7) the twinning stress is expected to be 11 kg/mm^2 for a Cu-alloy with SFE $\sim$ 50 ergs/cm^2. However, since the twinning in the Cu-alloys studied by Venables is by the $a/6 <11\bar{2}>\{111\}$ mode and the twinning in the fully ordered Cu_3Au is by the $a/3 <\bar{1}\bar{1}2>\{111\}$ mode, these stresses should not necessarily be comparable. Twinning stops after certain amounts of deformation. It is believed that twinning by the $a/3 <\bar{1}\bar{1}2>\{111\}$ mode occurs only when S is close to unity, and since S decreases as the alloy is deformed, the twinning should eventually stop.

Only $a/6 <11\bar{2}>\{111\}$ type twinning could occur in the Cu_3Au samples with $S \simeq 0$ and $S \simeq 0.5$ (Section 2.2). The SFE of these alloys is about 150 ergs/cm^2 (10), and the twinning stress is expected to be higher than 15 kg/mm^2 (7). The samples fractured before a stress high enough for twinning was reached, and no twinning was observed. The twinning stress for the $a/6 <11\bar{2}>\{111\}$ mode is expected to be even higher for the alloys with $S \simeq 0.9$ and $S \simeq 1.0$; therefore, this type of twinning does not occur when these alloys are deformed under uniaxial tension. Plane-strain compression studies were carried out in order to achieve stresses high enough to produce twins.

4.2 Rolling of Cu_3Au Single Crystals

The {111} pole figures of rolled Cu_3Au crystals for three different reductions are given in Figures 12-15. The intensity contours are plotted for n = 10, 20, 30, 40... etc., where n = 20 Ln (I+1.01); I is intensity. For the same amount of reduction, little differences in texture are observed for two different deformation temperatures.

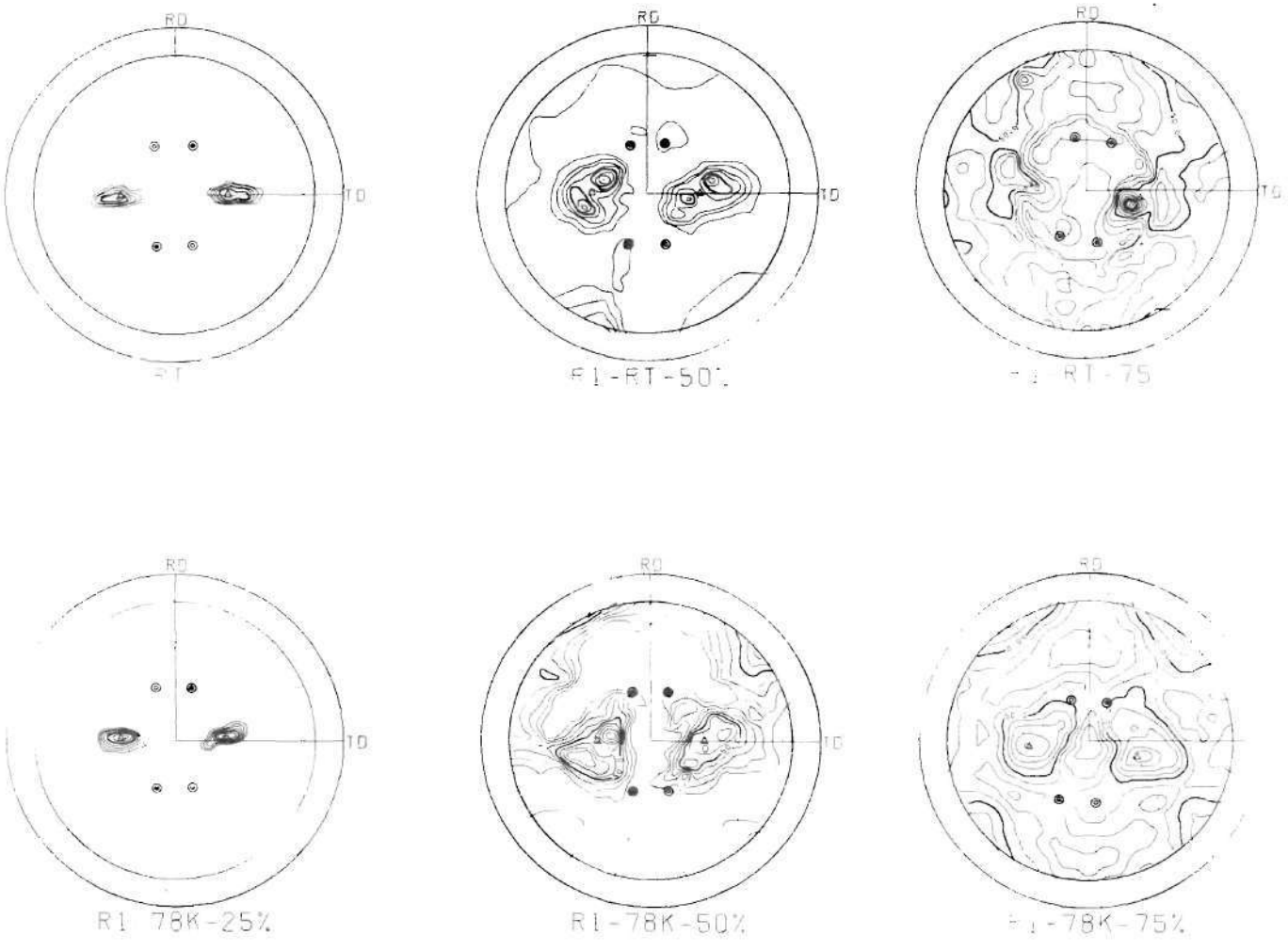

Figure 12. The (111) Pole Figures of Disordered Cu_3Au (R1) Rolled to 25 Percent, 50 Percent and 75 Percent at Room Temperature (RT) and at Liquid Nitrogen Temperature ($78^{o}K$).

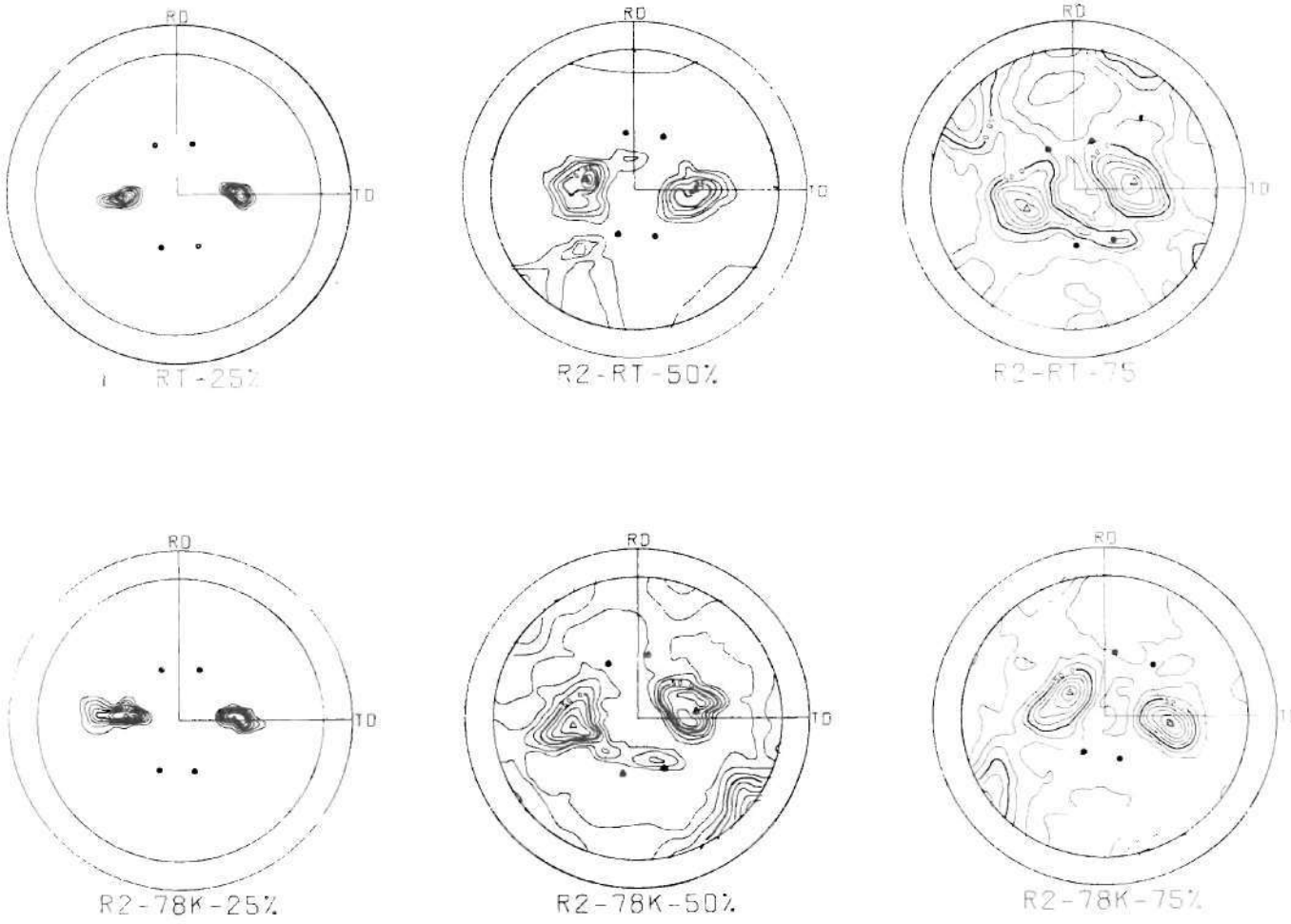

Figure 13. The (111) Pole Figures of Cu Au with S $\simeq$ 0.5 (R2) Rolled to 25 Percent, 50 Percent and 75 Percent at Room Temperature (RT) and at Liquid Nitrogen Temperature (78^{o}K).

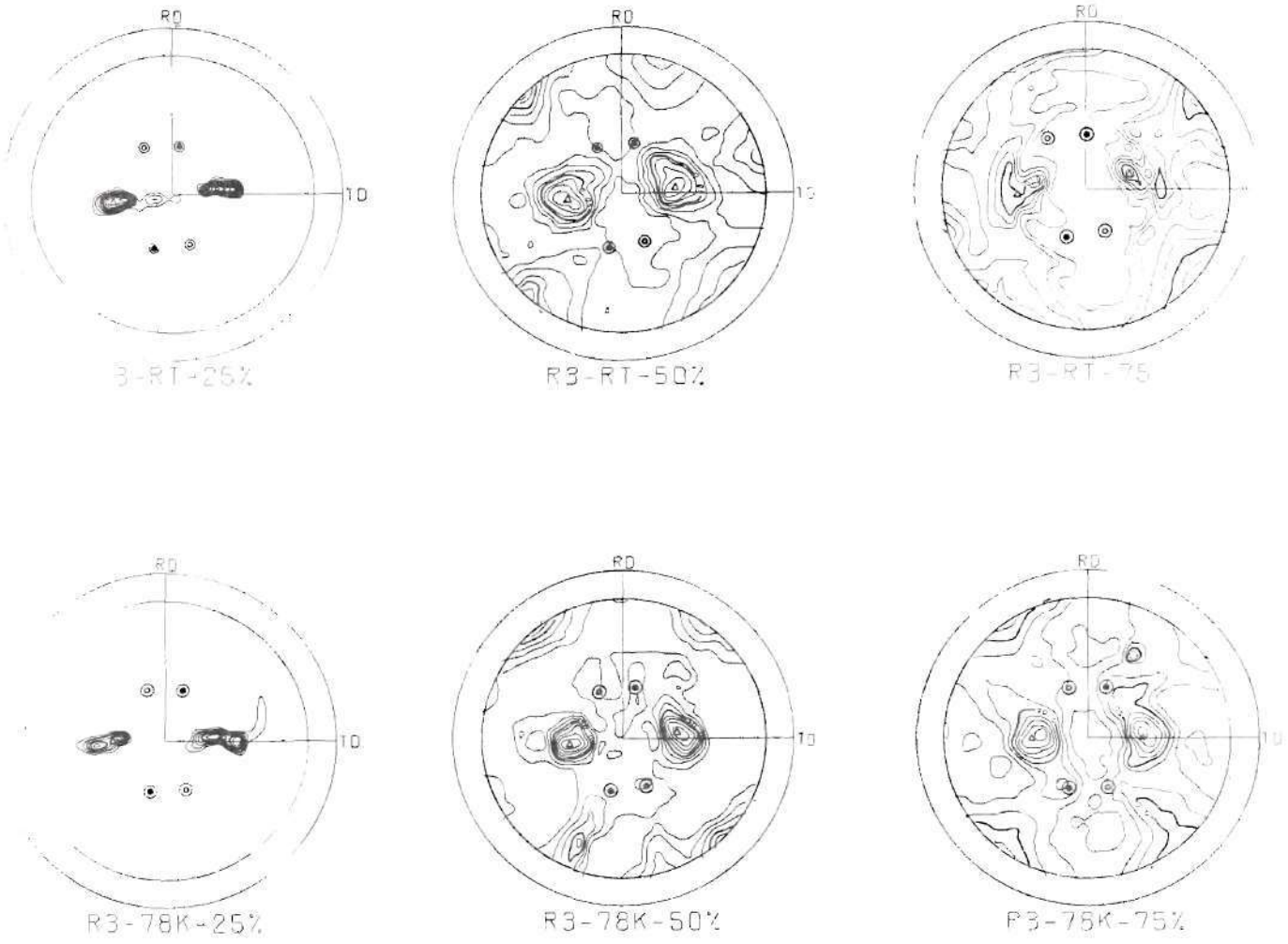

Figure 14. The (111) Pole Figures of Cu_3Au with S $\simeq$ 0.8 (R3) Rolled to 25 Percent, 50 percent and 75 percent at Room Temperature (RT) and at Liquid Nitrogen Temperature (78°K).

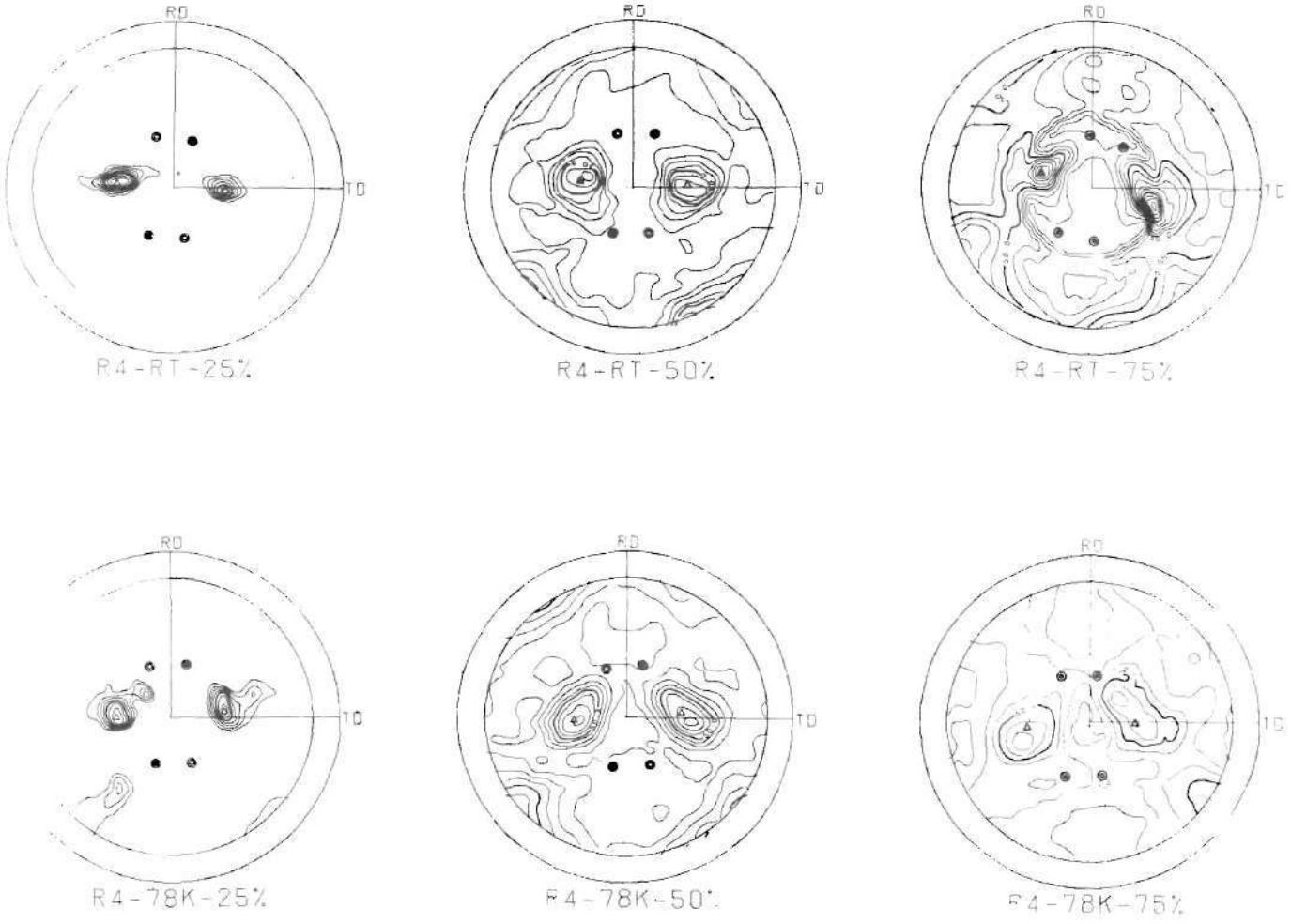

Figure 15. The (111) Pole Figures of Cu Au with $S \simeq 1.0$ (R4) Rolled to 25 Percent, 50 Percent and 75 Percent at Room Temperature (RT) and at Liquid Nitrogen Temperature (78°K).

Peaks are observed at some twin positions in some cases, as indicated in Table 4. In some cases, no twin peaks are observed even after 75% deformation, but this does not necessarily imply that deformation twinning does not occur. The deformation twins are highly distorted and may not be of sufficient volume to show a detectable peak. Also the twins may be reoriented during subsequent deformation before measurement of the texture, an idea which is supported by the observation that peaks which are present for R2-78^{o}K-50% almost disappeared after 25 percent additional deformation, Figure 13. The rotation of the twinned volume during the subsequent deformation is complex due to the additional constraints imposed by the surrounding matrix. However, it is conceivable that some rotation will take place due to the asymmetry of the orientation of the twins (110) rolling plane and [114] rolling direction .

From Table 4, it can be seen that the crystals also twin at room temperature, therefore for convenience, it was decided that plane strain compression studies would be carried out at room temperature. The plane-strain compression studies were necessary because, although rolling studies showed that twinning was possible at room temperature, twinning stresses could not be calculated. Rolling does not approximate plane-strain compression, because during rolling the flow direction could not be controlled accurately, and the dimensional increase in the cross-rolling direction leads to problems in the calculation of τ_t.

4.3 Plane Strain Compression Studies

Figure 16 shows the stress-strain (σ_{xx} - ϵ_{xx}) relationship of Cu_3Au crystals, with various initial degrees of long range order,

Table 4. Pole Figure Results of Rolled Cu_3Au Single Crystals with the (110) Rolling Plane and the [$1\bar{1}0$] Rolling Direction.

Sample Number	Deformation Temperature	Approximate Deformation,%	Results of Pole Figure Studies*
R1	78°K	25	0
		50	0
		75	1
	298°K	25	0
		50	1
		75	1
R2	78°K	25	0
		50	1
		75	1
	298°K	25	0
		50	0
		75	1
R3	78°K	25	0
		50	1
		75	1
	298°K	25	0
		50	0
		75	0
R4	78°K	25	0
		50	0
		75	1
	298°K	25	0
		50	0
		75	1

* 0 No twin peaks observed

1 Twin peaks are present

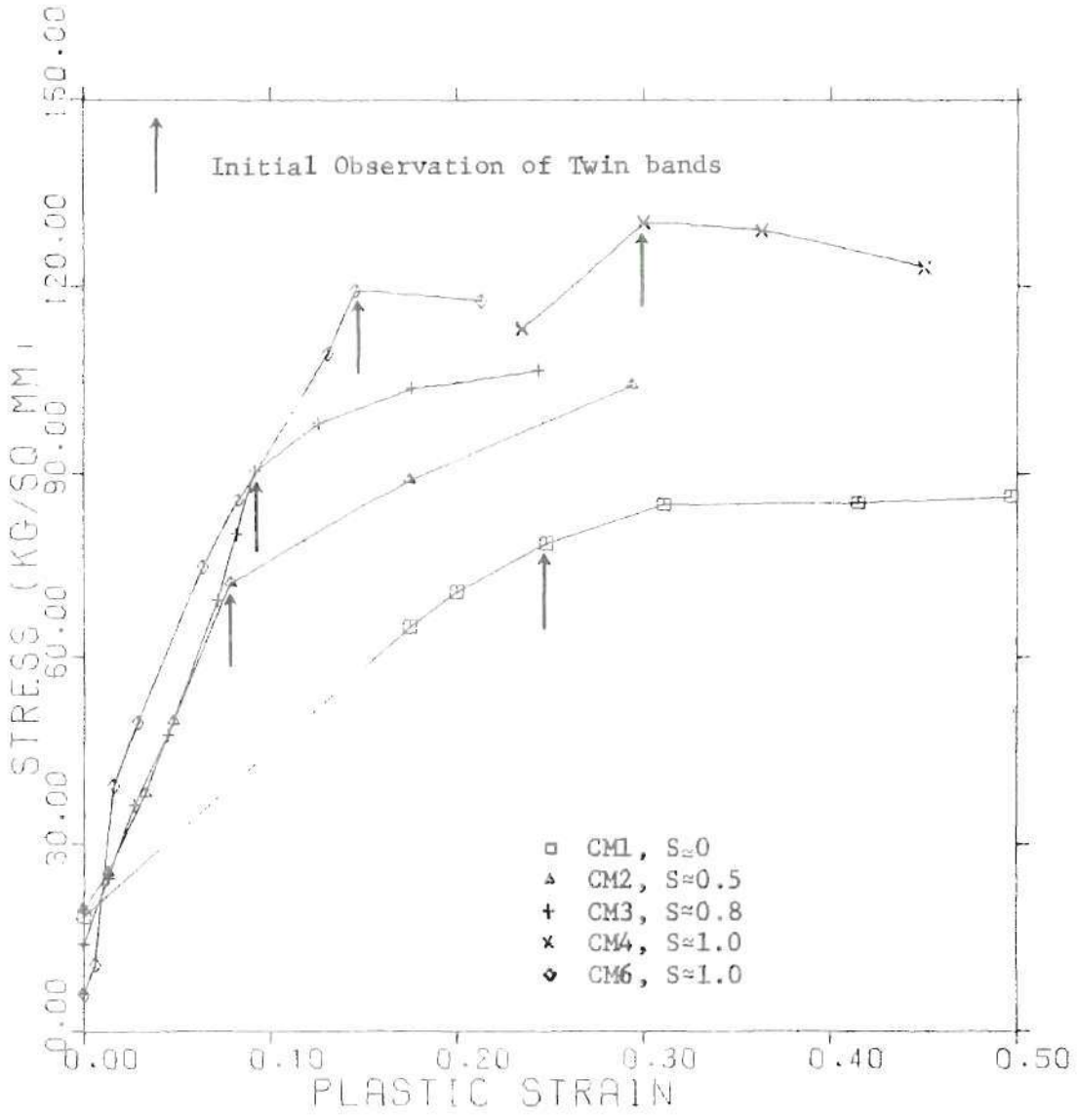

Figure 16. Stress-Strain (σ_{xx}-ε_{xx}) Curves of Cu_3Au with Various Degrees of Long Range Order Deformed Under Plane-Strain Compression with (110) Compression Plane and $[1\bar{1}0]$ Flow Direction. (CM1, CM2, CM3 and CM4 are Deformed at a Strain Rate of 1.5×10^{-3} and CM6 at 5×10^{-3}.)

deformed under plane strain compression. The deformation marks on the surface of the crystals were observed optically. It was found that broad bands appeared on the surface along $(\bar{1}11)$ and $(\bar{1}\bar{1}\bar{1})$ planes concurrently with changes in the slope of the stress strain curves. These bands are shown in Figures 17-20. These bands reappear after polishing and etching. They resemble the twin bands observed for a Cu-8% Fe alloy deformed at room temperature (16) and are composed of microtwins. These microtwins can be observed in the electron transmission micrographs shown in Figures 21-24. The changes in slope in stress-strain curves occur when the twinning on the a/6 $[\bar{1}12](\bar{1}11)$ systems start, since twinning relieves internal strain and lowers the stress for flow. Figure 25 shows the resolved shear stresses for twinning (τ_t) calculated from the σ_{xx} values at the onset of twinning, by a method described in Appendix B. τ_t initially decreases slightly and then increases rapidly, with S. The dynamic recovery becomes more and more difficult and deformation twinning becomes easier as S is increased, until S becomes quite large, then the effect of the change in neighbor relationship becomes pronounced (Section 2.2), causing a drastic increase in the value of τ_t. σ_{xx} for the fully ordered Cu_3Au specimens decreased as the samples were further deformed after the onset of twinning (Figure 16). The order parameter, and therefore the value of τ_t, decreases as the alloy is deformed, thereby lowering σ_{xx}.

The stress-strain curve for the silver single crystal deformed under (110) $[\bar{1}10]$ plane-strain compression is given in Figure 26. This curve appears similar to those of Cu_3Au (Figure 16). The pole-figure studies made after the curve changed slope show that the crystal

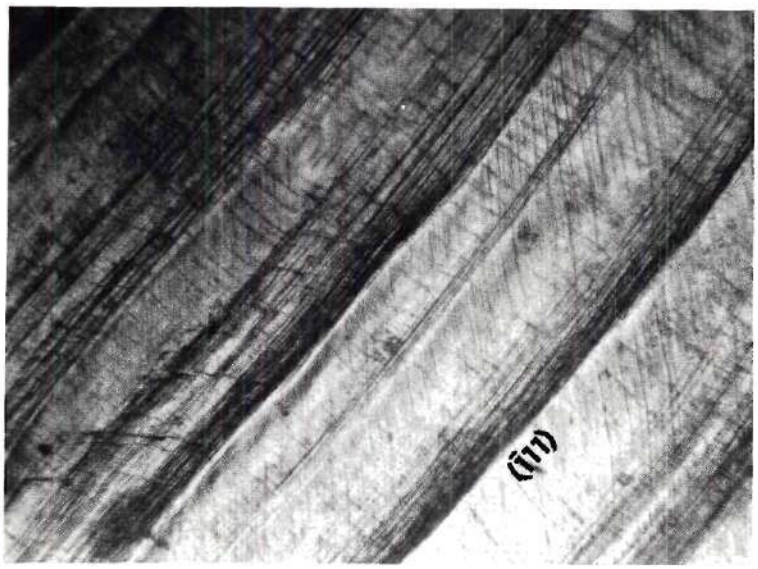

Figure 17. Optical Micrograph of the Surface of CM1 ($S \simeq 0$) at ϵ_{xx} = 0.415 (The specimen previously was polished at ϵ_{xx} = 0.311. The broad bands contain microtwins. The Fine markings are slip lines of different {111} planes. Magnification 110X.)

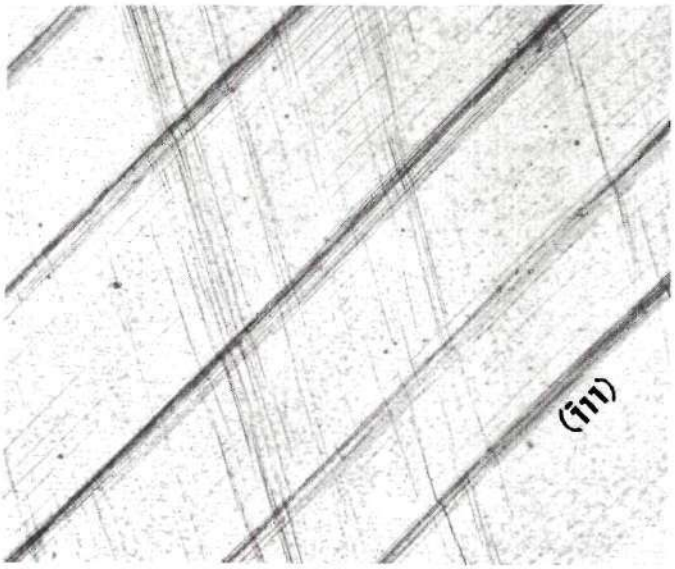

Figure 18. Optical Micrograph of the Surface of CM2($S \simeq 0.5$) at ϵ_{xx} = 0.079. (The specimen was previously polished at ϵ_{xx} = 0.033. The broad bands contain microtwins. The fine markings are slip lines on different {111} planes. Magnification 110X).

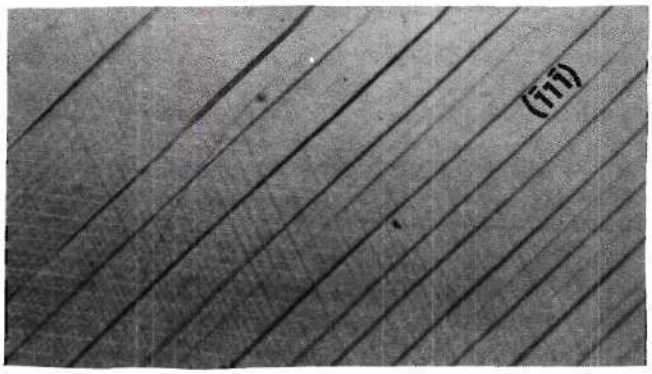

Figure 19. Optical Micrograph of the Surface of CM3 ($S \simeq 0.8$) at $\varepsilon_{xx} = 0.126$. (The specimen was previously polished at $\varepsilon_{xx} = 0.027$. The dark bands are twins and fine markings are slip lines on different $\{111\}$ planes. Magnification 75X.)

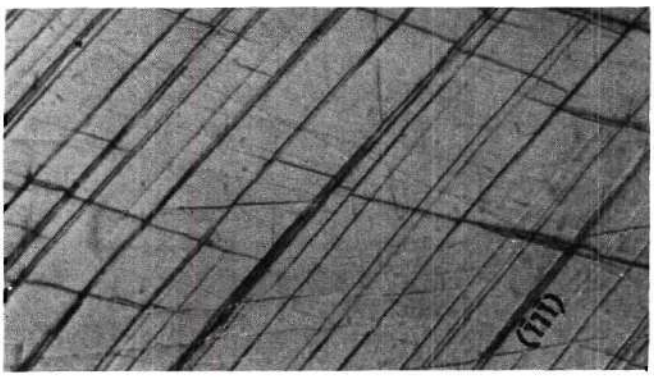

Figure 20. Optical Micrograph of the Surface of CM4 ($S \simeq 1.0$) at $\varepsilon_{xx} = 0.45$. (The specimen was previously polished at $\varepsilon_{xx} = 0.363$. The bands parallel to the trace of $(\bar{1}11)$ planes are composed of microtwins. Magnification 400X.)

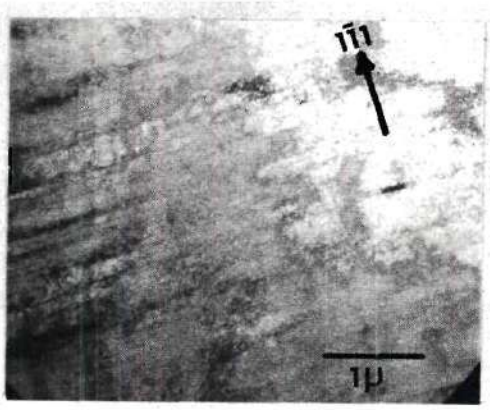

Figure 21. Electron Micrograph of CM1 ($S \simeq 0$) at $\epsilon_{xx} = 0.497$. Plane of the Micrograph is (112). (Bands formed parallel to $(1\bar{1}1)$ planes are due to the microtwins on these planes.)

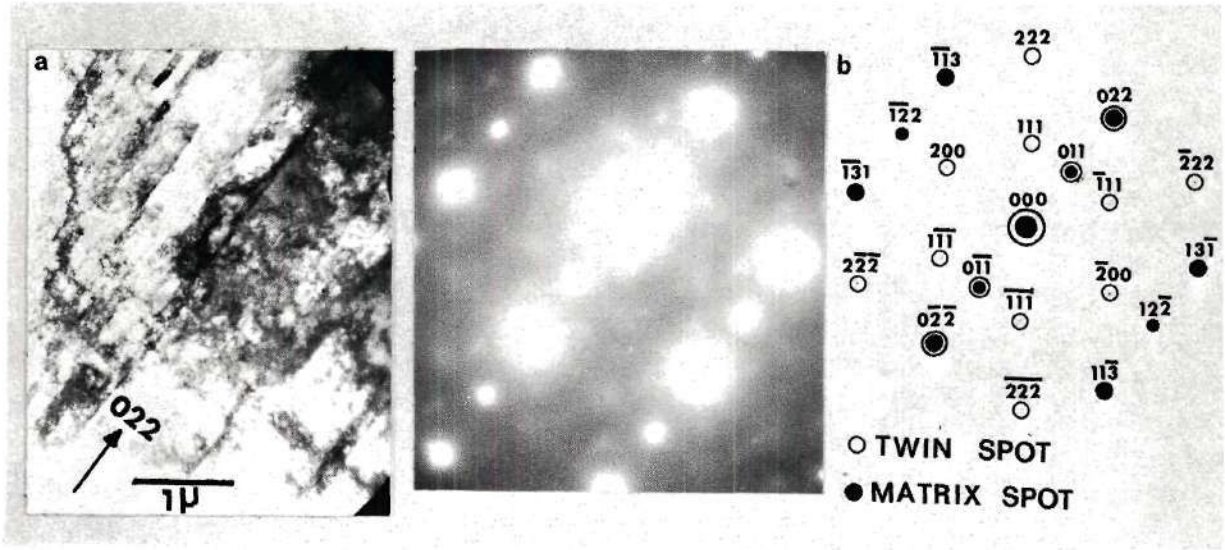

Figure 22. Electron micrographs of CM2 ($S \simeq 0.5$) at $\epsilon_{xx} = 0.297$.

((a) Band formation due to microtwins on the $(1\bar{1}1)$ planes. Plane of the micrograph is $(4\bar{1}1)$.

(b) The corresponding electron diffraction pattern. In this pattern $0\bar{1}1$ twin pattern is also present. $4\bar{1}1$ when operated with the $(1\bar{1}1)$ twin matrix produces $0\bar{1}1$, i.e. $[0\bar{1}1] = M\ [4\bar{1}1]$. Due to buckling of the foil matrix 100 pattern also can be seen.)

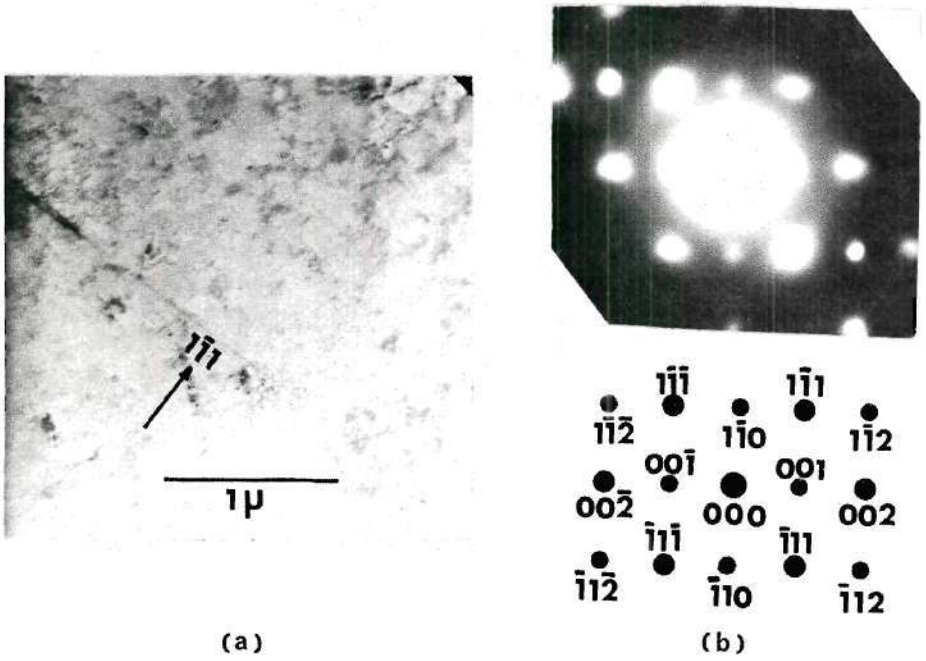

Figure 23. Transmission micrographs of CM3 ($S \simeq 0.8$) at $\varepsilon_{xx} = 0.244$.

((a) A bright field micrograph. The plane of the micrograph is (110).

(b) Corresponding electron diffraction pattern. Some streaking parallel to [111] and [111] directions, indicating presence of microtwins or stacking faults, can be seen. No twin spots can be seen because of small volume fraction of the twin.)

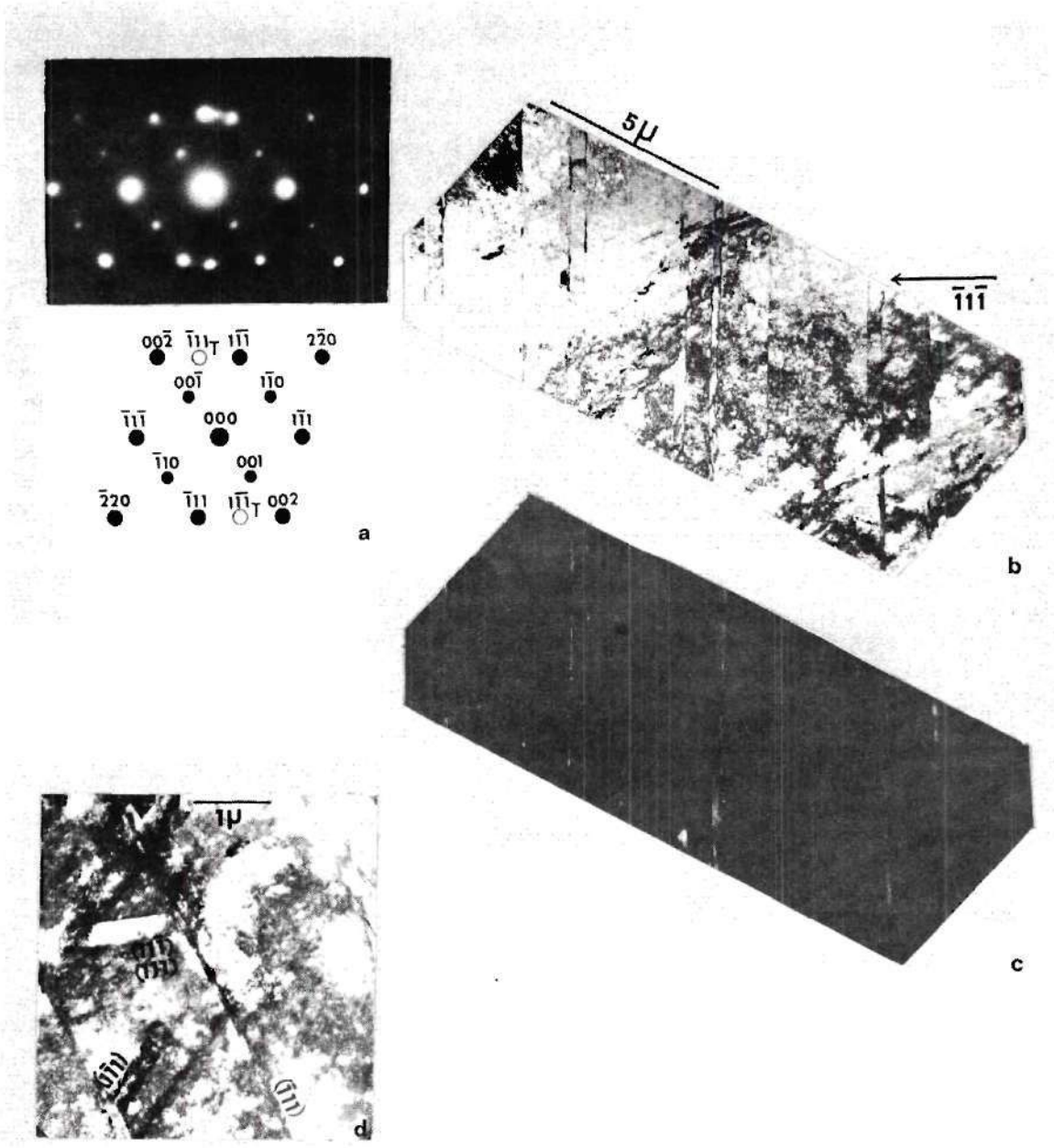

Figure 24. Transmission Micrographs of CM4 ($S \simeq 1$) at $\epsilon_{xx} = 0.363$.

((a) 110 electron diffraction pattern.
(b) Bright field micrograph. Plane of the micrograph is (110).
(c) Dark field micrograph with $\bar{1}11_T$ spot. The twins appear bright.
(d) Bright field micrograph of another area of the same foil. The plane of micrograph is (110). Twins on all four {111} planes can be seen.)

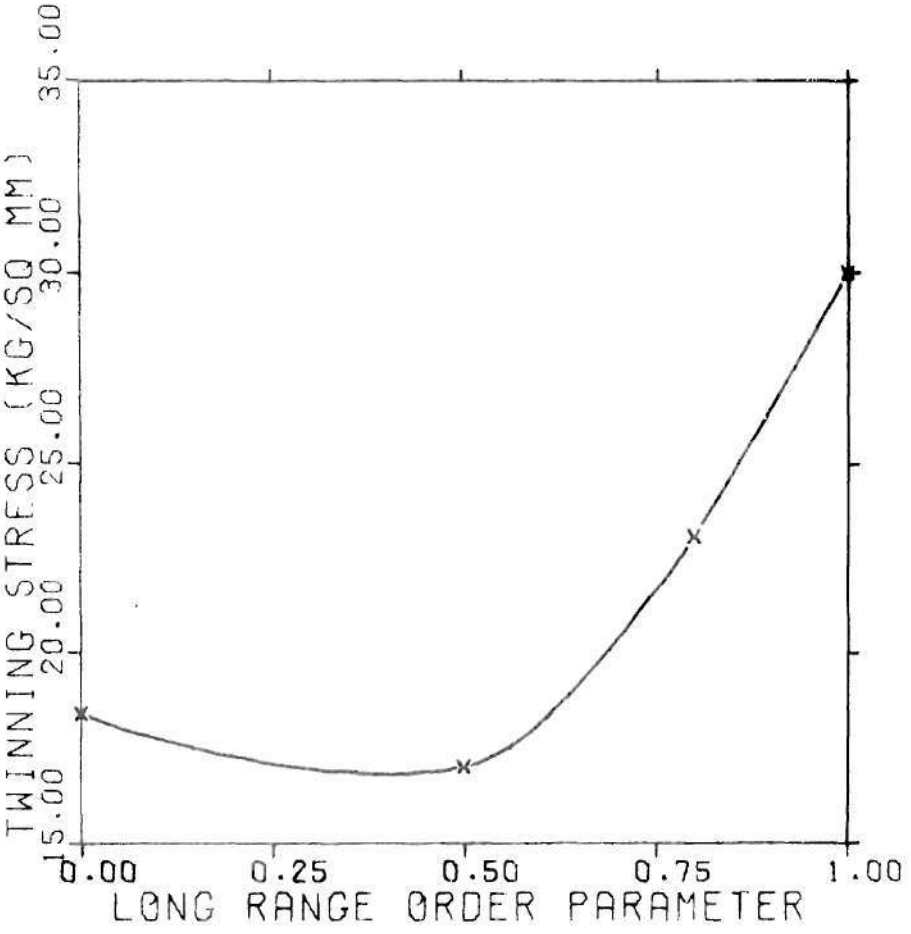

Figure 25. The Critical Resolved Shear Stress (τ) for Twinning, by the $(111)(11\bar{1})[11\bar{2}][112]$ 0.707 mode, of Cu_3Au with various degrees of Long Range Order.

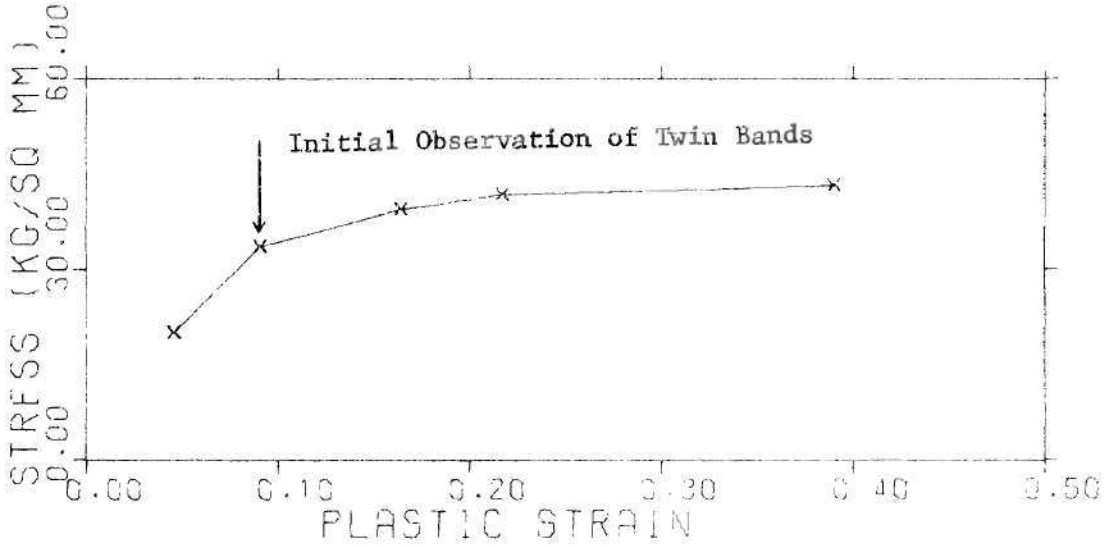

Figure 26. The Stress-Strain (σ_{xx} - ϵ_{xx}) Curve for Silver Deformed Under Plane Strain Compression with (110) Compression Plane and [$\bar{1}$10] Flow Direction.

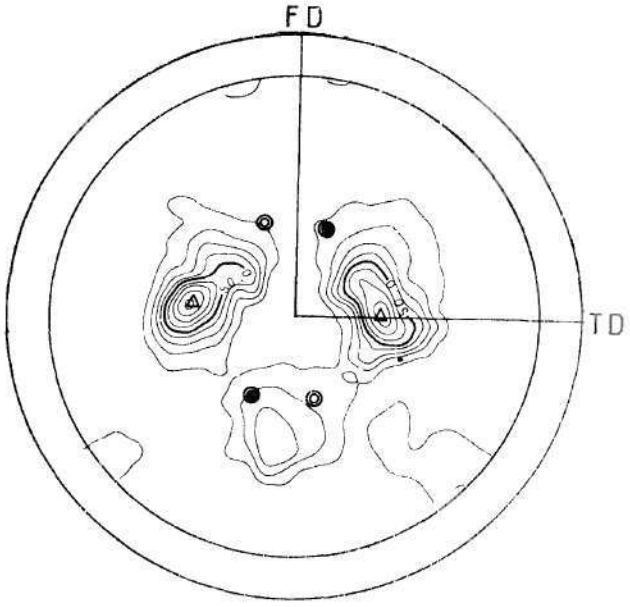

Figure 27. The (111) Pole Figure of the Silver Single Crystal at ϵ_{xx} = 0.39 Deformed Under (110) [$\bar{1}$10] Plane-Strain Compression.

contain twins (Figure 27). The curve changed slope indicating the onset of twinning at the σ_{xx} of about 35 kg/mm^2. This corresponds to τ_t of approximately 8 kg/mm^2, which is in good agreement with the tensile test results on silver single crystals reported by Suzuki and Barrett (37), viz. 7.81 and 7.35 kg/mm^2 for deformation at 193^{o}K and 273^{o}K, respectively.

In the electron micrographs of the completely ordered Cu_3Au specimens (Figure 24) twins are observed on all four {111} planes. It is believed that twinning occurs on the $(11\bar{1})$ and (111) planes by a/3 $[\bar{1}\bar{1}2]$ shear at a very early stage of deformation, when the order parameter is very close to unity. The required stress (τ_t') for twinning by the a/3 $\langle\bar{1}\bar{1}2\rangle\{111\}$ mode is 2.6 kg/mm^2, as obtained from tensile test results. Therefore, from case (c) of Table 2, twinning on a/3 $[\bar{1}\bar{1}2](11\bar{1})$ and a/3 $[\bar{1}\bar{1}2](111)$ systems should occur at a σ_{xx} of about 11 kg/mm^2. This stress is reached at a very early stage of the deformation of the completely ordered specimens. As the deformation continues S decreases and this mode of twinning stops. After further deformation the stress is raised to a high enough value and twinning occurs on the $(\bar{1}1\bar{1})$ and $(\bar{1}11)$ planes by the a/6 $[11\bar{2}]$ (111) mode. Thus twins on all four {111} planes are present in these specimens.

The interaction of twinning with existing slip bands and of slip with the existing twin bands, observed in all Cu_3Au specimens, are similar to those previously reported for a Co-8% Fe alloy (38). When the existing slip bands are sheared by twinning, the slip traces are displaced from their original position. The matrix slip propagates across the matrix-twin interface on an {111} plane of the twin.

From the transmission electron microscopy results (Figure 22 - 24), it can be seen that an appreciable proportion of order remains even after deformation under the (110) $[1\bar{1}0]$ plane-strain compression. However, the degree of order has been reported to decrease drastically when polycrystalline Cu_3Au is rolled (13) or shock-loaded (14). The rolled Cu_3Au single crystals also retained a large proportion of long range order even after they were deformed 75 percent. Polycrystalline Cu_3Au becomes disordered when rolled to such an extent (13); therefore, the change in S depends not only on the strain rate, but also on the orientation of the crystals.

4.4 Texture Results

The pole figures of the Cu_3Au single crystals deformed under (110) $[1\bar{1}0]$ plane strain compression are shown in Figures 28-31. Although twins were expected to be present in all cases, twin reflections were observed only in Figure 28(a) and 30(a). In all other cases the texture measurements were performed at stages of deformation long after the start of twinning. Twins are not observed in the pole-figures probably for the following reasons: When twins are formed after large deformations, they are small and highly distorted and their reflections are smeared; and when they are further deformed after their formation, the positions of their peaks are changed. The result is that small distorted twins of varying orientations are present in these alloys; but, their reflections are lost in the background.

Although twin reflections are not observed in some cases, the rotation of the matrix due to the twinning shear (Section 2.4) can be

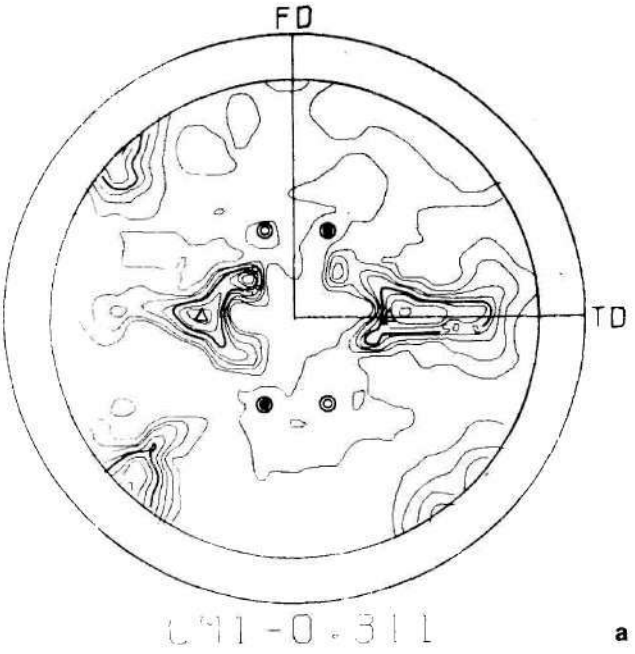

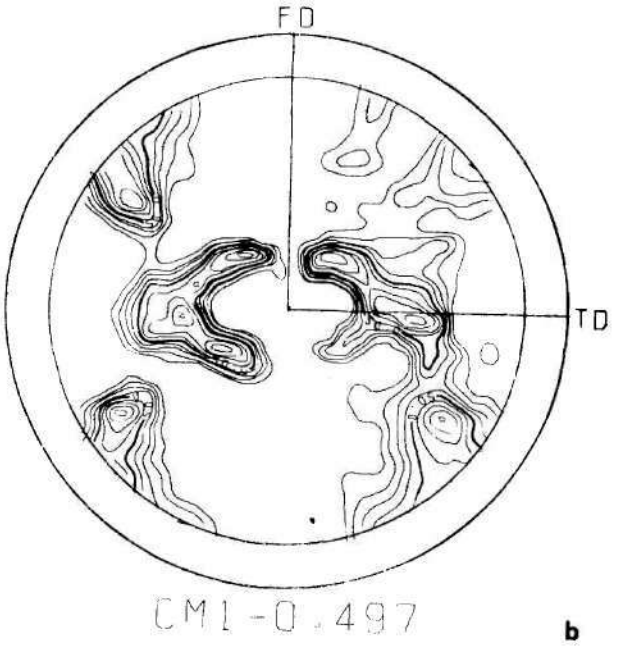

Figure 28. The {111} Pole Figures of CM1 ($S \simeq 0$) at

((a) $\epsilon_{xx} = 0.311$

(b) $\epsilon_{xx} = 0.497$)

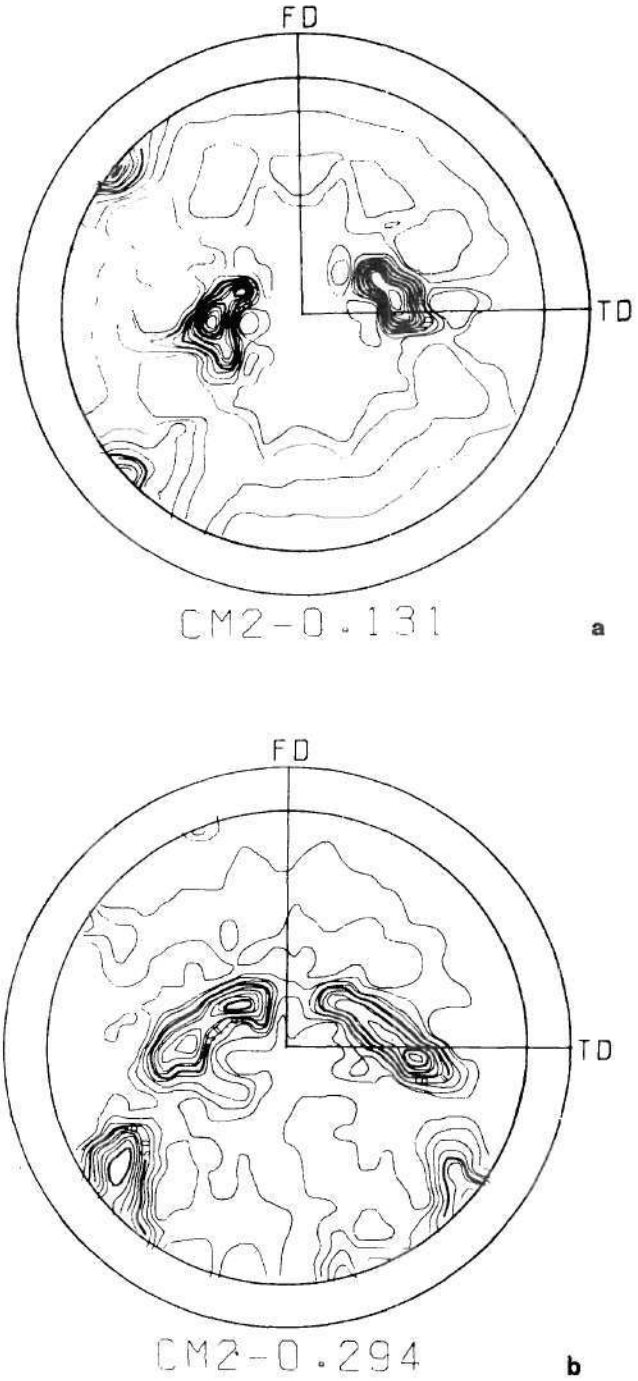

Figure 29. The {111} Pole Figures of CM2 ($S \simeq 0.5$) at

((a) $\epsilon_{xx} = 0.131$

(b) $\epsilon_{xx} = 0.294$)

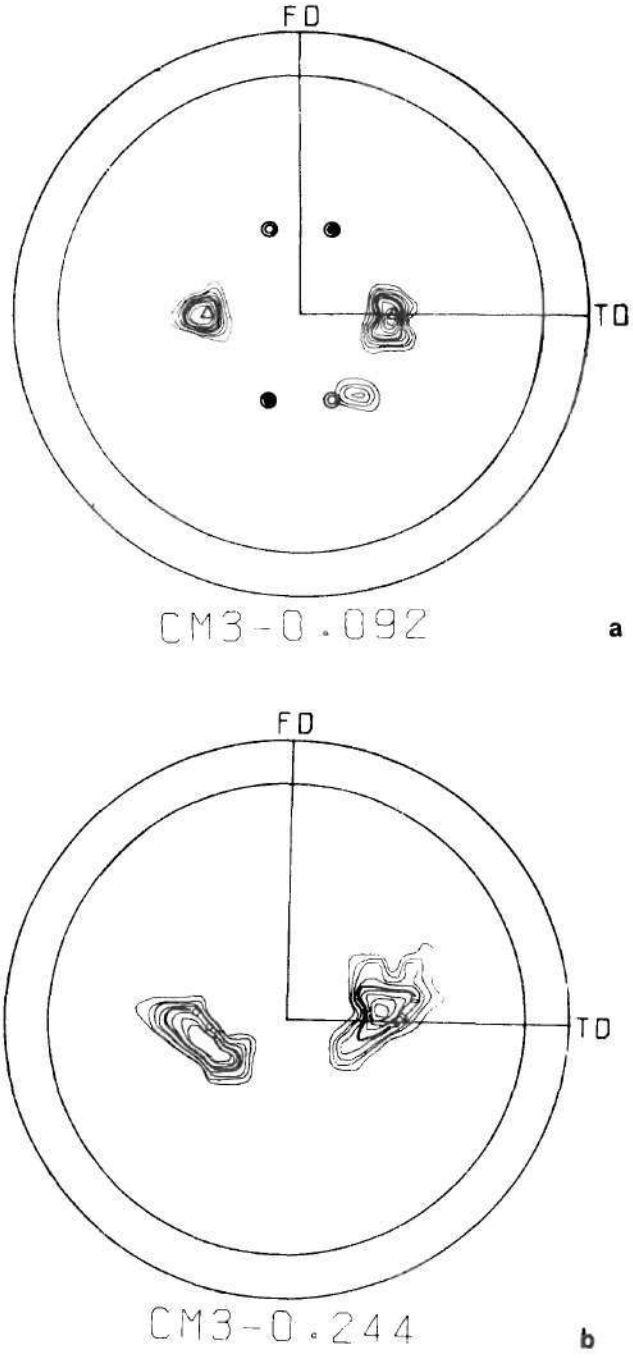

Figure 30. The {111} Pole Figures of CM3 ($S \simeq 0.8$) at

((a) $\epsilon_{xx} = 0.092$

(b) $\epsilon_{xx} = 0.244$)

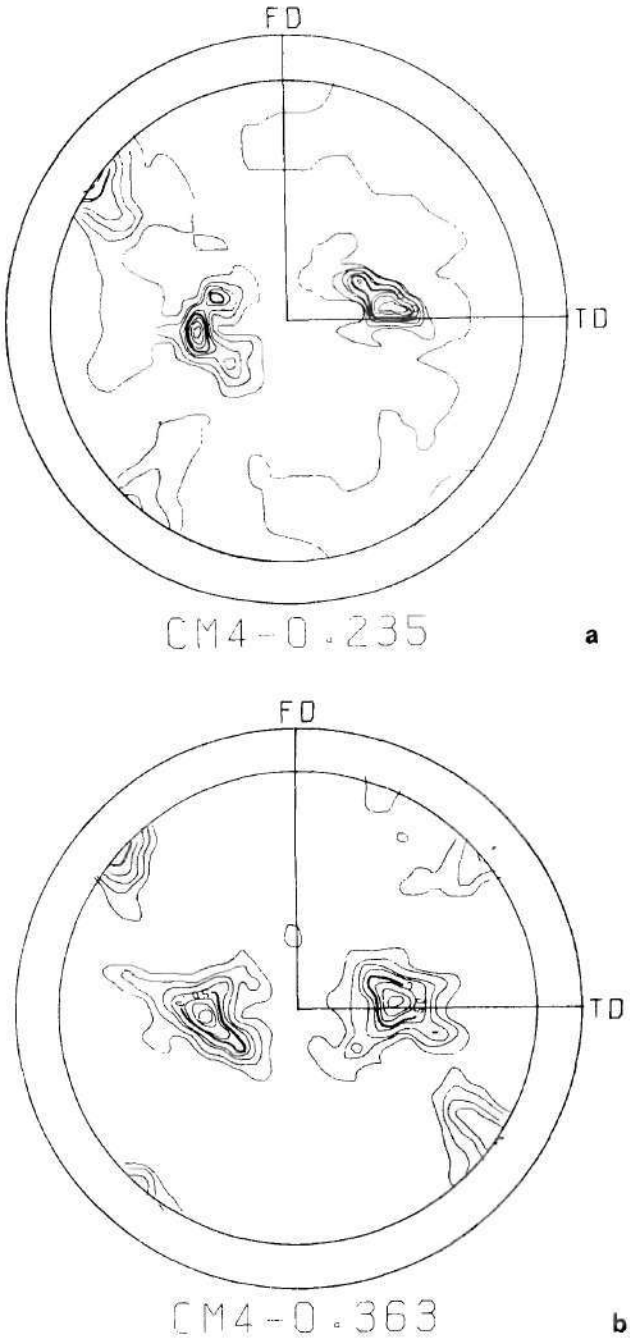

Figure 31. The {111} Pole Figures of CM4 ($S \simeq 1.0$) at

((a) $\epsilon_{xx} = 0.235$

(b) $\epsilon_{xx} = 0.363$)

observed in all of the pole figures. To illustrate such a rotation, the positions of the matrix {111} poles obtained from the predictions in Section 2.4 are superimposed on the pole figures presented in Figure 28(b); and the result is shown in Figure 32. The predicted positions and actual positions match quite well. In different areas of the same crystal, the change in orientation due to different twinning shears is such that the crystal effectively becomes polycrystalline. Figure 33 shows the polished and etched surface of the disordered Cu_3Au crystal deformed under plane-strain compression. It can be seen that the specimen is no longer a single crystal, since different areas have different orientations.

It should be noted here that the change in orientation discussed above is the same for twinning and faulting on the a/6 $\langle\bar{1}1\bar{2}\rangle$ $\{\bar{1}11\}$systems. However, the amount of deformation by faulting is limited, because it is not possible for faulting to occur more than once on the same plane. On the other hand, twinning and deformation of the twins after they are formed can account for a large extent of deformation. Therefore, the probable reason for the observed rotation is twinning and not faulting.

4.5 Twinning in Cu_3Au

Whenever the total internal stress at a point on a twin plane is increased above a certain limit, deformation twinning will start to relieve the stress, if other dislocation mechanisms (such as cross-slip, climb, etc.) cannot relieve the stress. This critical value of the stress will depend on the material and the operating twinning mode. The critical shear stress for twinning by the (111)(001)[$\bar{1}\bar{1}$2][110] 1.414

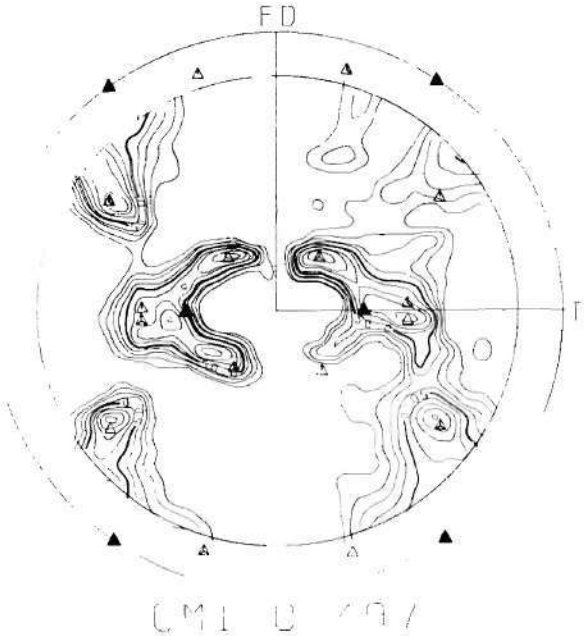

Figure 32. The {111} Pole Figures of CM1 ($S \simeq 0$) at $\varepsilon_{xx} = 0.497$, Superimposed on the Predicted Positions of the {111} Poles, Rotated due to Extensive Deformation on the 1/6 <112>{111} Systems (Section 2.4).

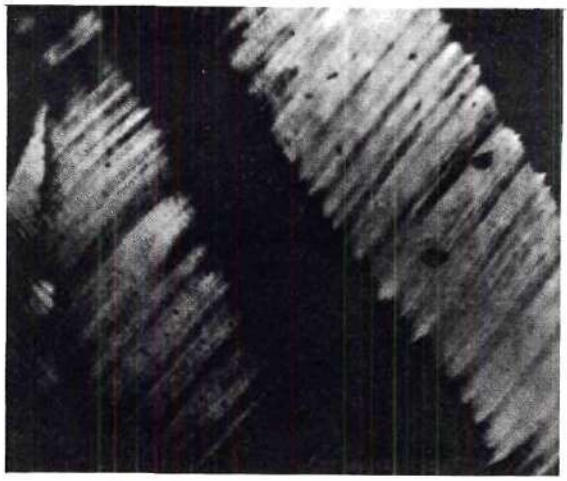

Figure 33. The Electropolished and Etched Surface of CM1 ($S \simeq 0$) at $\varepsilon_{xx} = 0.497$ as Viewed by Polarized Light. (The dark and bright areas are the portions of the crystal rotated differently. The crystal has effectively become polycrystalline due to the rotations and so the slope of the etched surface changes from one portion to another. The polarized microscopy distinguishes these differences in slopes. Magnification 33X.)

twinning mode for completely ordered Cu_3Au is very low. (The applied stress (τ_t') required for this type of twinning in the completely ordered Cu_3Au deformed under uniaxial tension, is given by $\tau_t'/G \sim 0.5 \times 10^{-3}$ whereas τ_t/G for Cu is $\sim 3.5 \times 10^{-3}$(39)). This mode is inoperative when the order parameter is less than one. The critical stress for twinning by the $(111)(11\bar{1})$ $[11\bar{2}][112]$ 0.707 mode increases with the long range order parameter in Cu_3Au due to the crystallographic restrictions imposed by the order. Twins are not produced by this mode in Cu_3Au specimens deformed under uniaxial tension, regardless of the degree of order or favorable orientation. However, this type of twinning is possible when these specimens are deformed under $(110)[1\bar{1}0]$plane-strain compression. The applied shear stress (τ_t) at which the twinning starts decreases slightly when the order parameter is initially increased, then increases rapidly as the order parameter is further increased. Dynamic recovery becomes difficult as the order parameter is increased; therefore, when the order parameter is initially increased, the internal stress required for twinning is reached at a slightly smaller stress (τ_t). The effect of crystallographic restrictions becomes prominent as the order parameter is further increased and τ_t consequently increases.

CHAPTER V

CONCLUSIONS

1. Twinning may occur in Cu_3Au by one of two modes, viz. (111)(001) $[\bar{1}\bar{1}2][110]$ 1.414 and (111)$(11\bar{1})[11\bar{2}][112]$ 0.707, depending upon the degree of long range order.

2. Completely ordered Cu_3Au twins by the (111)(001) $[\bar{1}\bar{1}2][110]$ 1.414 mode, and the critical resolved shear stress for twinning is low ($\tau_t'/G \sim 0.5 \times 10^{-3}$).

3. The completely ordered Cu_3Au twins with audible clicks at an early stage of deformation under uniaxial tension, along a direction close to <111>.

4. Disordered and partially ordered Cu_3Au twin by the (111) $(11\bar{1})[11\bar{2}][112]$ 0.707 mode and the shear stress for twinning increases with the degree of long range order, due to the crystallographic restrictions imposed by the order.

5. Disordered and partially ordered Cu_3Au do not twin when deformed under uniaxial tension; but they do twin when deformed under (110) $[1\bar{1}0]$ plane-strain compression.

6. The degree of long range order of the initially completely ordered Cu_3Au decreases with deformation, and twinning by the (111)$(11\bar{1})$ $[11\bar{2}][112]$ 0.707 mode becomes possible by (110) $[1\bar{1}0]$ plane-strain compression.

7. The only significant effect of twinning on the texture of

Cu_3Au single crystals was found to be the rotation of the matrix due to the twinning shear.

APPENDIX A

CHANGE IN THE NEAREST NEIGHBOR RELATIONSHIP ACROSS THE MATRIX TWIN INTERFACE

The Nearest Neighbors in the Matrix of Cu_3Au with Long Range Order Parameter S.

In face centered cubic lattice, a unit cell contains one corner site and three face-centered sites. Corner site has 12 face-centered sites as nearest neighbors. The nearest neighbors of face-centered sites are 4 corner sites and 8 face-centered sites.

Probability that a face-centered site is occupied by a Cu atom, $P^{Cu}_{1/2} = \frac{S+3}{4}$.

Probability that a corner site is occupied by a Cu atom, $P^{Cu}_{0} = \frac{3-3S}{4}$.

Probability that a corner site is occupied by an Au atom, $P^{Au}_{0} = \frac{3S+1}{4}$.

Probability that a face-centered site is occupied by an Au atom, $P^{Au}_{1/2} = \frac{1-S}{4}$.

Then, the number of nearest neighbor Cu atoms around a corner site, $N^{Cu}_{0} = 12\ P^{Cu}_{1/2} = 9 + 3S$,

the number of nearest neighbor Cu atoms around a face-centered site, $N^{Cu}_{1/2} = 8\ P^{Cu}_{1/2} + 4\ P^{Cu}_{0} = 9-S$,

the number of nearest neighbor Au atoms around a corner site, $N^{Au}_{0} = 12\ P^{Au}_{1/2} = 3 - 3S$, and

the number of nearest neighbor Au atoms around a face-centered site, $N^{Au}_{1/2} = 8\ P^{Au}_{1/2} + 4\ P^{Au}_{0} = 3 + S$.

Fraction of Cu atoms in face-centered sites, $f^{Cu}_{1/2} = \frac{3P^{Cu}_{1/2}}{3} \quad \frac{S+3}{4}$

Fraction of Cu atoms in corner sites, $f^{Cu}_{o} = 1 - f^{Cu}_{1/2} = \frac{1-S}{4}$

Fraction of Au atoms in face-centered sites, $f^{Au}_{1/2} = 3P^{Au}_{1/2} = \frac{3-3S}{4}$

Fraction of Au atoms in corner sites, $f^{Au}_{o} = 1-f^{Au}_{1/2} = \frac{3S+1}{4}$

The average number of nearest neighbor Au atoms around a Cu atom, $(Cu^{Au})_M = f^{Cu}_{1/2} \cdot N^{Au}_{1/2} + f^{Cu}_{o} \cdot N_o{}^{Au} = S^2 + 3$.

The average number of nearest neighbor Cu atoms around an Au atom, $(Au^{Cu})_M = f^{Au}_{1/2} \cdot N^{Cu}_{1/2} + f^{Au}_{o} \cdot N^{Cu}_{o} = 3S^2 + 9$.

<u>The Nearest Neighbors in the Twin Formed by the a/6 $\langle 11\bar{2} \rangle \{111\}$ mode</u>.

Twinning changes the positions of matrix atoms as shown in Figure 4. The face-centered site on the a or b planes (α or β sites) has 8 matrix face-centered atoms and 4 matrix corner atoms as nearest neighbors. The face site on the c planes (γ site) and the corner site (c site) have 10 matrix face-centered atoms and 2 matrix corner atoms as nearest neighbors. The α and β sites are filled by matrix face-centered atoms and γ and c sites are filled 50 per cent by matrix corner atoms and 50 per cent by matrix face-centered atoms.

Then,

the fraction of Cu atoms occupying α and β sites, $f^{Cu}_{\alpha\beta} = 2/3\ P^{Cu}_{\frac{1}{2}} = \frac{S+3}{6}$

the fraction of Cu atoms occupying γ and c sites, $f^{Cu}_{\gamma c} = 1-f^{Cu}_{\alpha\beta} = \frac{3-S}{6}$

the fraction of Au atoms occupying α and β sites, $f^{Au}_{\alpha\beta} = 2\,P^{Au}_{\frac{1}{2}} = \frac{1-S}{2}$

the fraction of Au atoms occupying γ and c sites, $f^{Au}_{\gamma c} = 1-f^{Au}_{\alpha\beta} = \frac{1+S}{2}$

and,

the number of Cu nearest neighbors of α and β sites, $N^{Cu}_{\alpha\beta} = 8\,P^{Cu}_{1/2} + 4\,P^{Cu}_{o}$,

the number of Au nearest neighbors of α and β sites, $N^{Au}_{\alpha\beta} = 8\,P^{Au}_{1/2} + 4\,P^{Au}_{o}$,

the number of Cu nearest neighbors of γ and c sites, $N^{Cu}_{\gamma c} = 10\,P^{Cu}_{1/2} + 2\,P^{Cu}_{o}$, and

the number of Au nearest neighbors of γ and c sites, $N^{Au}_{\gamma c} = 10\,P^{Au}_{1/2} + 2\,P^{Au}_{o}$.

The average number of nearest neighbor Au atoms around a Cu atom, $(Cu^{Au})_T = f^{Cu}_{\alpha\beta} \cdot N^{Au}_{\alpha\beta} + f^{Cu}_{\gamma c} \cdot N^{Au}_{\gamma c} = 3 + \frac{S^2}{3}$

The average number of nearest neighbor Cu atoms around an Au atom, $(Au^{Cu})_T = f^{Au}_{\alpha\beta} \cdot N^{Cu}_{\alpha\beta} + f^{Au}_{\gamma c} \cdot N^{Cu}_{\gamma c} = 9+S^2$.

The Change in Number of Nearest Neighbors Due to Twinning

The decrease in the average number of nearest neighbor Cu atoms around an Au atom = $(Au^{Cu})_M - (Au^{Cu})_T = 2S^2$.

The decrease in the average number of nearest neighbor Au atoms around a Cu atom = $(Cu^{Au})_M - (Cu^{Au})_T = \frac{2\,S^2}{3}$.

APPENDIX B

CALCULATION OF τ_t

The critical resolved shear stress for twinning by the a/3 {111} $\langle 11\bar{2} \rangle$ mode can be calculated from the compression stress at the onset of twinning during deformation by plane-strain compression. Twinning by 1/6 <112> shear occur on $(\bar{1}1\bar{1})$ and $(\bar{1}11)$ planes when α is less than or equal to $2/\sqrt{3}$ (Section 2.3). The value of α at the onset of twinning is $2/\sqrt{3}$. The corresponding M is $2\sqrt{6}$.

The twinning stress is given by

$$\tau_t = \alpha \cdot (\tau_s)_t = \frac{2}{\sqrt{3}} \cdot \frac{(\sigma_{xx})t}{M} = \frac{(\sigma_{xx})t}{4.24}$$

where $(\sigma_{xx})_t$ is the compressive stress at the onset of twinning, and $(\tau_s)_t$ is the resolved shear stress for slip at the onset of twinning.

BIBLIOGRAPHY

1. G. Wasserman, Z. Metallkunde 54 (1963) 61.

2. F. Haessner, Z. Metllkunde 54 (1963) 98.

3. I. L. Dillamore, and W. T. Roberts, Acta Met., 12 (1964), 281.

4. R. E. Smallman, and D. Green, Acta Met. 12 (1964), 145.

5. H. Hu, R. S. Cline, and S. R. Goodman, in Recrystallization, Grain Growth and Textures, Ed., H. Margotin, Amer. Soc., Metals, Metals Park, Ohio (1966), 295.

6. Mahajan, and Williams, International Met. Rev., 18 (1973), 43.

7. J. A. Venables, in Deformation Twinning, Ed., R. E. Reed-Hill, Gordon and Breach Sci. Publ., N. Y. (1964), p. 77.

8. D. E. Mikkola, and J. B. Cohen, J. Appl. Phys. 33 (1962), 892.

9. M. J. Marcinkowski, and L. Zwell, Acta Metl. 11 (1963), 373.

10. A. Camazi, G. Schianch and E. Rimini, Phil. Mag. 16 (1967) 1207.

11. F. Laves, Naturwiss. 39 (1952) 546.

12. R. W. Cahn and J. A. Coll, Acta Met. 9 (1961), 138.

13. E. A. Starke, Jr., J. C. Ogle and C. J. Sparks, Jr., Adv. X-ray Analysis 12 (1969), 372.

14. D. E. Mikkola and J. B. Cohen, Acta Met., 14 (1966), 105.

15. T. H. Blewitt, R. R. Coltman, and J. K. Redman, J. Appl. Phys., 28 (1957), 651.

16. G. Y. Chin, W. F. Hosford, and D. R. Mendorf, Proc. Roy. Soc., A309 (1969), 433.

17. N. S. Stoloff and R. G. Davis, Prog. Mat. Sci., 13 (1966), 3.

18. R. G. Davis, and N. S. Stoloff, Phil. Mag., 12 (1965), 297.

19. R. G. Davis, and N. S. Stoloff, Phil. Mag., 9 (1964), 349.

20. B. H. Kear, Acta Met., 12 (1964), 555.

21. B. H. Kear, Acta Met., 14 (1966), 659.

22. G. W. Ardley, Acta Met., 3 (1955), 525.

23. B. H. Kear, A. F. Griamei, G. R. Leverant, and J. M. Oblak, Scripta Met., 3 (1969), 123.

24. B. H. Kear, A. F. Griamei, G. R. Leverant, and J. M. Oblak, Scripta Met., 3 (1969), 455.

25. M. J. Marcinkowski, and D. S. Miller, Phil. Mag., 6 (1961), 871.

26. V. S. Arunachalam, and C. M. Sargent, Scripta Met., 5 (1971), 949.

27. B. H. Kear, J. M. Oblak, and A. F. Griamei, in Proceedings of the Second International Conference on Strength of Metals and Alloys, ASM, Metals Park, Ohio (1970), 1155.

28. A. Guimier, and J. L. Strudel, ibid., p. 1145.

29. G. I. Taylor, J. Inst. Metals. 62 (1938), 307.

30. S. Mahajan, Metallography, 4 (1971), 43.

31. M. Sakai, and D. E. Mikkola, Met Trans. 2 (1971), 1635.

32. D. R. Chipman, J. Appl. Phys., 27 (1956), 739.

33. E. W. Horne, M.S. Thesis, Georgia Institute of Technology (1969).

34. G. Y. Chin, E. A. Nesbitt, and A. J. Williams, Acta Met., 14 (1966), 487.

35. J. E. Gragg, Jr., P. Bardhan, and J. B. Cohen, in Critical Phenomena in Alloys, Magnets and Superconductors, Ed., R. E. Mills, E. Ascher, and R. I. Jaffee, McGraw-Hill, New York (1971).

36. J. B. Cohen, J. Met. Sci., 4 (1969), 1012.

37. H. Suzuki, and C. S. Barrett, Acta Met., 6 (1958), 156.

38. S. Mahajan and G. Y. Chin, Acta Met., 21 (1973), 173.

39. P. R. Thornton and T. E. Mitchell, Phil. Mag., 7 (1962), 361.

VITA

Saghana Baran Chakrabortty, the son of Dr. and Mrs. P. K. Chakrabortty, was born in Midnapore, India on July 28, 1948. He graduated from Hamilton High School, Tamluk, India in 1964. In July, 1964, he entered the Indian Institute of Technology, Kharagpur, India and received a Bachelor's degree in Metallurgical Engineering there in June, 1969.

He came to the Graduate Division of the Georgia Institute of Technology in September, 1969 and received a Master of Science in Metallurgy in June, 1971.